Article

Young CSF restores oligodendrogenesis and memory in aged mice via Fgf17

https://doi.org/10.1038/s41586-022-04722-0

Received: 20 May 2021

Accepted: 4 April 2022

Published online: 11 May 2022

Check for updates

Tal Iram[1,2]✉, Fabian Kern[1,3,4], Achint Kaur[1,2], Saket Myneni[1,2], Allison R. Morningstar[1,2], Heather Shin[1,2], Miguel A. Garcia[5], Lakshmi Yerra[6], Robert Palovics[1,2], Andrew C. Yang[1,2], Oliver Hahn[1,2], Nannan Lu[1,2], Steven R. Shuken[1,2,7], Michael S. Haney[1,2], Benoit Lehallier[1,2], Manasi Iyer[5], Jian Luo[1,6], Henrik Zetterberg[8,9,10,11], Andreas Keller[1,3,4,12], J. Bradley Zuchero[5] & Tony Wyss-Coray[1,2,13]✉

Recent understanding of how the systemic environment shapes the brain throughout life has led to numerous intervention strategies to slow brain ageing[1–3]. Cerebrospinal fluid (CSF) makes up the immediate environment of brain cells, providing them with nourishing compounds[4,5]. We discovered that infusing young CSF directly into aged brains improves memory function. Unbiased transcriptome analysis of the hippocampus identified oligodendrocytes to be most responsive to this rejuvenated CSF environment. We further showed that young CSF boosts oligodendrocyte progenitor cell (OPC) proliferation and differentiation in the aged hippocampus and in primary OPC cultures. Using SLAMseq to metabolically label nascent mRNA, we identified serum response factor (SRF), a transcription factor that drives actin cytoskeleton rearrangement, as a mediator of OPC proliferation following exposure to young CSF. With age, SRF expression decreases in hippocampal OPCs, and the pathway is induced by acute injection with young CSF. We screened for potential SRF activators in CSF and found that fibroblast growth factor 17 (Fgf17) infusion is sufficient to induce OPC proliferation and long-term memory consolidation in aged mice while Fgf17 blockade impairs cognition in young mice. These findings demonstrate the rejuvenating power of young CSF and identify Fgf17 as a key target to restore oligodendrocyte function in the ageing brain.

Brain ageing underlies dementia and neurodegenerative diseases, imposing an immense societal burden. Systemic interventions in model organisms have shown great promise in reversing ageing-related decline of various tissues, including the brain[1]. For example, heterochronic parabiosis and young plasma transfer rejuvenated the aged brain and restored memory function[2,3]. Nevertheless, the brain is protected with barriers, which may limit access to these factors, presumably impeding their rejuvenation potential. Cerebrospinal fluid (CSF), which is in close association with brain cells, carries signals that instruct neuronal progenitor proliferation and specification during development[6]. However, CSF protein composition changes with human ageing[7], marked by an increase in inflammatory proteins[8] and a decrease in growth factors such as brain-derived neurotrophic factor (BDNF)[9]. Whether these changes in CSF contribute to age-related cognitive decline is unknown. Testing this functionally by performing CSF transfers in vivo has been difficult owing to technical limitations in CSF collection and direct CSF infusion to the brain. We theorized that intracerebroventricular (ICV) administration of young CSF to aged mice would have rejuvenating effects on the brain (Fig. 1a).

Regulation of oligodendrogenesis by young CSF

We first sought to test whether infusion of young CSF into aged mice could improve ageing-related impairments in hippocampal-dependent learning and memory tasks[10]. Twenty-month-old mice received three foot shocks associated with a tone and a flashing light. Mice were then randomly split into two groups and infused with either artificial CSF (aCSF) or young mouse CSF (YM-CSF) for 1 week and remote memory recall was tested 3 weeks after memory acquisition. YM-CSF infusion resulted in higher average freezing rates following exposure to the tone and light, suggesting better preservation of the remote fear memory (Fig. 1b). We selected this paradigm because it allowed us to test interventions that affect remote memory formation and consolidation[11], a process implicated in ageing-related cognitive decline[12]. Notably, aged

[1]Department of Neurology and Neurological Sciences, Stanford University School of Medicine, Stanford, CA, USA. [2]Wu Tsai Neurosciences Institute, Stanford University School of Medicine, Stanford, CA, USA. [3]Clinical Bioinformatics, Saarland University, Saarbrücken, Germany. [4]Department of Clinical Bioinformatics, Helmholtz Institute for Pharmaceutical Research Saarland (HIPS)–Helmholtz Centre for Infection Research (HZI), Saarland University Campus, Saarbrücken, Germany. [5]Department of Neurosurgery, Stanford University School of Medicine, Palo Alto, CA, USA. [6]Palo Alto Veterans Institute for Research, Palo Alto, CA, USA. [7]Department of Chemistry, Stanford University, Stanford, CA, USA. [8]Department of Psychiatry and Neurochemistry, Institute of Neuroscience and Physiology, Sahlgrenska Academy at the University of Gothenburg, Mölndal, Sweden. [9]Clinical Neurochemistry Laboratory, Sahlgrenska University Hospital, Mölndal, Sweden. [10]Department of Neurodegenerative Disease, UCL Institute of Neurology, Queen Square, London, UK. [11]UK Dementia Research Institute at UCL, London, UK. [12]Center for Bioinformatics, Saarland Informatics Campus, Saarbrücken, Germany. [13]Paul F. Glenn Center for the Biology of Aging, Stanford University School of Medicine, Stanford, CA, USA.
✉e-mail: tal.iram@stanford.edu; twc@stanford.edu

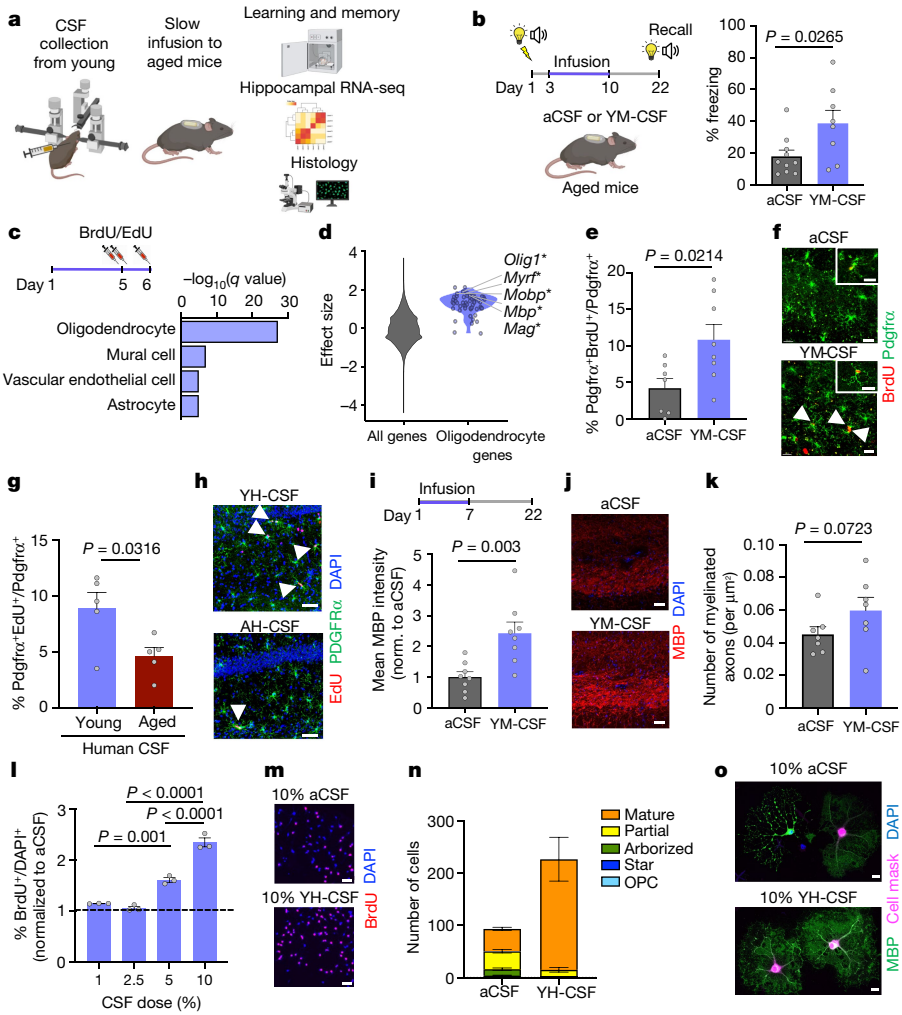

Fig. 1 | Young CSF improves memory consolidation and promotes OPC proliferation and differentiation. a, Overview of the experimental paradigm. **b**, Percentage of freezing for 20-month-old mice in the remote recall contextual fear conditioning test (aCSF, $n = 10$; YM-CSF, $n = 8$; two-sided t test; mean ± s.e.m.). **c**, GSEA of hippocampal bulk RNA-seq data identifies oligodendrocyte genes as highly upregulated following 6 d of infusion with YM-CSF. **d**, Effect size of oligodendrocyte genes in the hippocampus of mice infused with YM-CSF versus aCSF compared with all genes in the dataset (an asterisk indicates FDR < 0.1) (aCSF, $n = 8$; YM-CSF, $n = 7$). **e**, Quantification of proliferating OPCs in the hippocampus following 6 d of aCSF or YM-CSF infusion into 20-month-old mice (aCSF, $n = 7$; YM-CSF, $n = 8$; two-sided t test; mean ± s.e.m.). **f**, Representative images of the experiment in **e**. Arrowheads point to proliferating OPCs. Scale bars, 20 µm (insets, 5 µm). **g**, As in **e** but for YH-CSF and AH-CSF ($n = 5$; two-sided t test; mean ± s.e.m.). **h**, Representative images of the experiment in **g**. Scale bars, 50 µm. **i**, Hippocampal MBP staining following the long-term paradigm of infusion with aCSF or YM-CSF ($n = 8$; two-sided t test; mean ± s.e.m.). **j**, Representative images of the experiment in **i**. Scale bars, 50 µm. **k**, Quantification of the number of myelinated axons per µm² in the hippocampus of aged mice following the long-term paradigm of infusion with aCSF or YM-CSF ($n = 7$; one-sided t test; mean ± s.e.m.). **l**, Ratio of the percentage of BrdU⁺/DAPI⁺ primary rat OPCs treated with the indicated dose of YH-CSF over matching aCSF as control ($n = 3$; one-way ANOVA followed by Tukey's post hoc test; mean ± s.e.m.). **m**, Representative images of the experiment in **l**. Scale bars, 50 µm. **n**, Stacked bar plots of the average number of cells in each differentiation state at day 4 of differentiation with 10% aCSF or 10% YH-CSF (aCSF, $n = 281$ cells analysed on 3 coverslips; YH-CSF, $n = 454$ cells analysed on 2 coverslips). **o**, Representative images of the experiment in **n**. Scale bars, 20 µm. See Supplementary Videos 1 and 2.

mice infused with aCSF had comparable freezing rates to age-matched naive mice (aCSF, 17.82% ± 0.93; naive, 17.73% ± 0.93; mean + s.e.m.). Because the hippocampus is central to age-related cognitive decline and is in close apposition to CSF, we measured the effect of infusion with young CSF on the hippocampal transcriptome by bulk RNA sequencing (RNA-seq). Differential gene expression analysis between mice infused with aCSF and YM-CSF identified 271 differentially expressed genes (DEGs) whose expression was significantly altered (false discovery rate (FDR) < 0.1) after treatment with young CSF, of which 115 genes were downregulated and 156 genes were upregulated (Supplementary Table 1). Notably, oligodendrocyte genes were highly upregulated, identifying this cell type as a major cellular substrate for CSF (Fig. 1c and Extended Data Fig. 1a, b). Specifically, young CSF promoted upregulation of transcription factors driving oligodendrocyte differentiation and major myelin protein components (for example, *Olig1*, *Myrf*, *Mag*, *Mbp* and *Mobp*) (Fig. 1d). In line with these findings, even acute single infusions of young CSF, but neither aCSF nor aged mouse CSF (AM-CSF), resulted in upregulation of these oligodendrocyte marker genes 16 h after injection (Extended Data Fig. 1c and Supplementary Table 2).

Neuronal activity, induced by optogenetic tools or by learning tasks, was shown to promote oligodendrocyte progenitor cell (OPC) proliferation and differentiation, as well as to regulate myelin plasticity in mature oligodendrocytes[13]. To determine whether OPC proliferation could be underlying the transcriptomic signature observed following infusion with young CSF, we labelled dividing cells in the last 2 d of young CSF infusion with thymidine analogues (BrdU or EdU). Interestingly, whereas overall cell proliferation was very low in these aged brains, we discovered a surge in overall cell proliferation specifically in

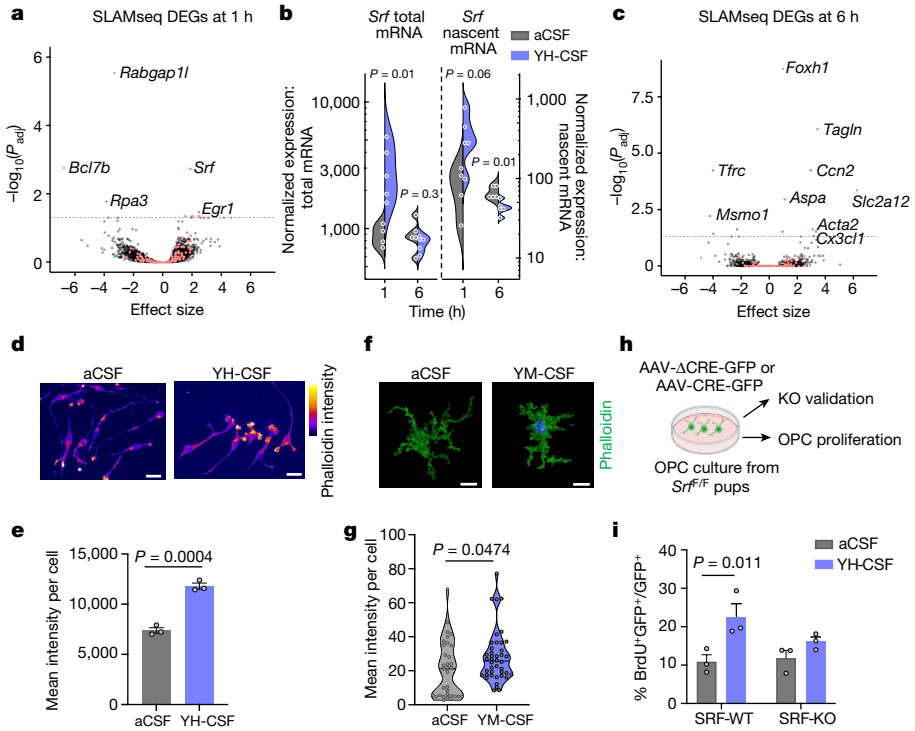

Fig. 2 | SRF is induced by young CSF and mediates CSF-induced OPC proliferation. a, Volcano plot of DEGs at 1 h following addition of YH-CSF (SRF targets in red) (YH-CSF 1 h, $n = 4$; rest, $n = 5$; adjusted P value obtained by Wald test in DESeq2; dashed line represents $P_{adj} = 0.05$). **b**, Normalized expression levels of *Srf* in nascent mRNA counts and total counts (YH-CSF 1 h, $n = 4$; rest, $n = 5$; two-way ANOVA with Sidak's post hoc test (nascent and total reads separately)). **c**, Volcano plot of DEGs at 6 h following addition of YH-CSF (SRF targets in red) ($n = 5$; adjusted P value obtained by Wald test in DESeq2; dashed line represents $P_{adj} = 0.05$). **d**, Representative images of the experiment in **e**. Scale bars, 20 µm. **e**, Mean phalloidin intensity in OPCs 6 h following exposure to YH-CSF ($n = 3$ coverslips per condition; two-sided t test; mean ± s.e.m.). **f**, Representative images of the experiment in **g**. Scale bars, 10 µm. **g**, Mean phalloidin intensity in hippocampal OPCs (Pdgfrα$^+$) following infusion with aCSF or YM-CSF for 6 d ($n = 3$ mice per group, total of 33–42 single cells measured per condition; two-sided t test; mean ± s.e.m.). **h**, Schematic of mouse OPC primary cultures from *Srf*$^{F/F}$ pups infected with AAVs encoding Cre–GFP to induce recombination or △Cre–GFP as a control. **i**, Percentage of proliferating cells (BrdU$^+$GFP$^+$/GFP$^+$) among SRF-WT and SRF-KO cells treated with 10% aCSF or YH-CSF ($n = 3$; two-way ANOVA followed by Sidak's post hoc test; mean ± s.e.m.).

the hippocampus, relatively distant from the infusion site (Extended Data Fig. 1d–i). Young CSF induced a 2.35-fold increase in the percentage of proliferating OPCs (platelet-derived growth factor receptor α (Pdgfrα)$^+$BrdU$^+$/Pdgfrα$^+$) in the CA1 region of the hippocampus but not in the cortex (Fig. 1e, f and Extended Data Fig. 2a–f). In an additional cohort of mice, we infused aged mice with human CSF pooled from healthy young donors (YH-CSF, mean age of 24.6 years) or aged donors (AH-CSF, mean age of 69 years). YH-CSF induced OPC proliferation at comparable levels to YM-CSF, whereas AH-CSF induced proliferation for only half as many cells (Fig. 1g, h). Notably, CSF infusions also triggered EdU incorporation in astrocytes and microglia (Extended Data Fig. 2g–i). Next, we allowed these proliferating cells to mature for 3 weeks to assess the effects of young CSF on hippocampal myelination by MBP staining and transmission electron microscopy (TEM). We found an increase in MBP intensity (Fig. 1i, j) and in the number of myelinated axons (Fig. 1k and Extended Data Fig. 3) in the molecular layer of the hippocampus. This indicates that young CSF contains signals that promote cell growth for the oligodendrocyte lineage or substances that neutralize inhibitory factors.

To assess whether young CSF can stimulate OPC proliferation and differentiation directly, we used an established primary rat OPC culture system[14]. Cells were grown in full proliferation medium supplemented with human CSF pools (three pools as replicates, with each pool from three young adult healthy males (YH-CSF, mean age of 24.6 years) or aCSF as a control). We used human instead of rodent CSF because this allowed us to obtain the much larger volumes necessary for these studies. Similarly to the in vivo infusions, BrdU pulsing studies confirmed a dose-dependent increase in OPC proliferation (Fig. 1l, m). Notably, when OPCs were deprived of mitogens to promote cell differentiation over 4 d, YH-CSF not only induced a twofold increase in cell survival—in a process in which a substantial fraction of cells typically undergo apoptotic cell death[15]—but also promoted prominent expansion of the more differentiated mature cell morphology[16] with an overall increase in MBP intensity per cell (Fig. 1n, o, Extended Data Fig. 4a, b and Supplementary Videos 1 and 2). These results are in line with previous work in which human CSF from young healthy donors was shown to induce neuronal viability[17], whereas CSF from individuals with multiple sclerosis was toxic to neuronal[18] and OPC[19] cultures.

SRF mediates the effects of young CSF on OPCs

To gain a deeper mechanistic understanding of the cellular processes induced by young CSF in OPCs, we metabolically labelled nascent mRNA with 4-thiouridine (s^{4}U) using thiol (SH)-linked alkylation for the metabolic sequencing of RNA (SLAMseq) from cultured OPCs 1 or 6 h after exposure to YH-CSF. The top gene induced after 1 h was for serum response factor (SRF) (Fig. 2a, Extended Data Fig. 5a–e and Supplementary Table 3), a transcription factor studied extensively in skeletal muscle[20], heart[21] and neurons in the brain[22]. SRF binds to serum response element (SRE) promoter sequences to induce cell motility, proliferation and differentiation through modulation of immediate early genes (such as *Egr1*) and the actin cytoskeleton[23]. We also noted marked downregulation of the genes encoding the negative regulator of Wnt signalling and pro-apoptotic factor Bcl7b and the

DNA repair protein Rpa3, in line with an overall prosurvival response following YH-CSF exposure. Nascent *Srf* mRNA transcripts peaked at 1 h and returned to baseline by 6 h (Fig. 2b). Notably, many of the DEGs peaking at 6 h are known SRF target genes (Fig. 2c, red). Indeed, the most strongly increased genes were enriched for 'target genes of SRF' on the basis of gene set enrichment analysis (GSEA) and the TRANSFAC database (Extended Data Fig. 5f), while the cells maintained OPC identity as determined by NG2 expression (Extended Data Fig. 4c, d). The combined $\log_2$-transformed fold change in TRANSFAC-predicted targets for SRF (423 genes), validated SRF targets (74 genes, curated list from the literature) and actin genes (212 genes) in the dataset indicated overall activation of the SRF pathway and actin cytoskeleton transcripts (Extended Data Fig. 5g and Supplementary Table 4). To test whether CSF-induced SRF expression regulates the OPC actin cytoskeleton, we exposed OPCs to YH-CSF in the presence of SiR-actin, a fluorescent probe used to label actin filaments for live imaging, or we fixed and stained OPCs with the actin filament dye phalloidin. SiR-actin intensity increased within hours of OPC stimulation with YH-CSF, without a change in total area, indicating an increase in cellular actin filament levels (Extended Data Fig. 6a–c). In fixed cells, OPCs exposed to YH-CSF for 6 h expressed twice as much phalloidin per cell as controls (Fig. 2d, e). The increase in phalloidin intensity was confirmed in hippocampal OPCs in aged mice infused with YM-CSF for 6 d (Fig. 2f, g).

Because SRF is necessary for the formation of actin filaments in axonal growth cones in neurons[24], we tested whether it has a similar role in OPCs and quantified the number of growth cones per OPC. We found that YH-CSF induced significantly more growth cones per cell compared with aCSF (Extended Data Fig. 6d). To test whether SRF is mediating the effect of young CSF, we infected cultured OPCs from mice with *loxP*-flanked *Srf* with adeno-associated viruses (AAVs) encoding Cre–GFP (to create SRF-knockout (SRF-KO) OPCs) or truncated Cre–GFP as a control (SRF-WT). We repeated the YH-CSF proliferation experiment and showed that CSF-induced proliferation is dependent on SRF (Fig. 2h, i and Extended Data Fig. 6e–i). These results shed light on the possible mechanisms underlying the effect of young CSF on OPCs and point towards SRF and actin cytoskeleton regulation as potential mediators of the effects of young CSF in vivo.

Deletion of SRF signalling specifically in muscle cells causes accelerated ageing phenotypes in the skeletal muscle of mice[25] and worms[26]. We thus asked whether SRF signalling may be downregulated in OPCs in the ageing brain. Indeed, the fraction of SRF-positive OPCs (SRF^+ $Pdgfr\alpha^+/Pdgfr\alpha^+$) in the CA1 region of the hippocampus detected by in situ hybridization decreased markedly with age (Fig. 3a, b). To expand this analysis to other SRF targets and cellular processes, we sorted hippocampal OPC and mature oligodendrocyte (OL) nuclei by expression of the gene encoding the oligodendrocyte transcription factor Olig2 ($Olig2^{high}$ for OPCs and $Olig2^{low}$ for OLs) from young (3-month-old) and aged (25-month-old) mice and performed bulk RNA-seq (Extended Data Fig. 7a, b and Supplementary Table 5). The top pathways downregulated in OPCs with ageing were related to oligodendrocyte cell markers, regulation of glial cell differentiation, cellular respiration and metabolism, and protein folding. Conversely, immune-related pathways and microglia-specific genes were upregulated with ageing, as previously reported for OPCs in ageing[27] and multiple sclerosis[28] (Fig. 3c, d and Extended Data Fig. 7c, d). A focused analysis of SRF TRANSFAC target genes in ageing OPCs indicated overall downregulation with age (Fig. 3e, left box plot).

We next aimed to test whether young CSF induces SRF pathway activation in vivo in the aged brain. Because of the transient nature of SRF induction in the SLAMseq experiment, we designed an acute injection paradigm where CSF was injected into the lateral ventricle of 18-month-old mice and contralateral hippocampi were dissected 1 and 6 h after injection for RNA-seq of OPC and OL nuclei (Supplementary Table 6). We found again that genes predicted to be targets of SRF (on the basis of TRANSFAC) were upregulated in OPCs at both time points

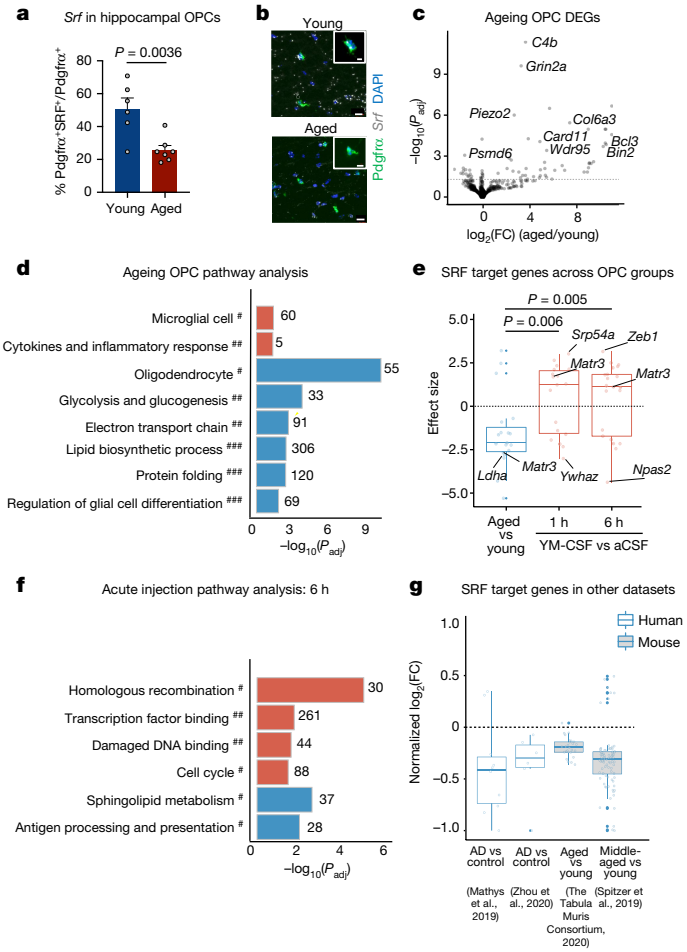

Fig. 3 | SRF signalling is downregulated in hippocampal OPCs with ageing and induced by acute injection of young CSF. a, *Srf* mRNA quantified in OPCs ($Pdgfr\alpha^+$ nuclei) in the CA1 region of the hippocampus of young (3 months) and aged (22 months) mice (young, $n = 6$; aged, $n = 7$; two-sided t test; mean ± s.e.m.). **b**, Representative images of the experiment in **a**. Scale bars, 10 µm (5 µm in insets). **c**, Volcano plot of DEGs of aged versus young hippocampal OPC nuclei. The dashed line represents $P_{adj} = 0.05$ ($n = 4$). FC, fold change. **d**, Pathways enriched (red) or depleted (blue) in hippocampal OPCs with age. Resource categories: #, CellMarker; ##, WikiPathways; ###, Gene Ontology Biological Processes ($n = 4$; numbers to the right of the bar represent number of genes identified in the category; unweighted Kolmogorov–Smirnow test). **e**, Box plots of the effect size of SRF targets (TRANSFAC database) in hippocampal OPCs from aged versus young mice and mice treated with YM-CSF versus aCSF at 1- and 6-h time points ($n = 4$; genes prefiltered by a cut-off of $P < 0.05$, Wilcoxon rank-sum test; boxes show the median and the 25th–75th percentile range, and whiskers indicate values up to 1.5 times the interquartile range; dashed line indicates effect size = 0). **f**, Pathways enriched (red) or depleted (blue) in hippocampal OPCs 6 h after injection with aCSF or YM-CSF ($n = 4$). Resource categories: #, KEGG; ##, Gene Ontology Molecular Function (numbers to the right of the bar represent number of genes identified in the category; unweighted Kolmogorov–Smirnow test). **g**, Meta-analysis of the $\log_2$-transformed fold change in expression of SRF target genes (TRANSFAC) in human AD versus control and mouse aged versus young ageing datasets[71–74] (genes prefiltered by a cut-off of $P < 0.05$; boxes show the median and 25th–75th percentile range, and whiskers indicate values up to 1.5 times the interquartile range; dashed line indicates normalized $\log_2(FC) = 0$).

(Fig. 3e and Extended Data Fig. 8a). At the 6-h time point, genes upregulated in OPCs were linked to SRF-related pathways such as 'regulation of GTPase activity', 'chromatin organization', 'transcription factor binding', 'cell cycle' and 'regulation of cytoskeleton organization' (Fig. 3f and Extended Data Fig. 8b–d). SRF target genes were also downregulated

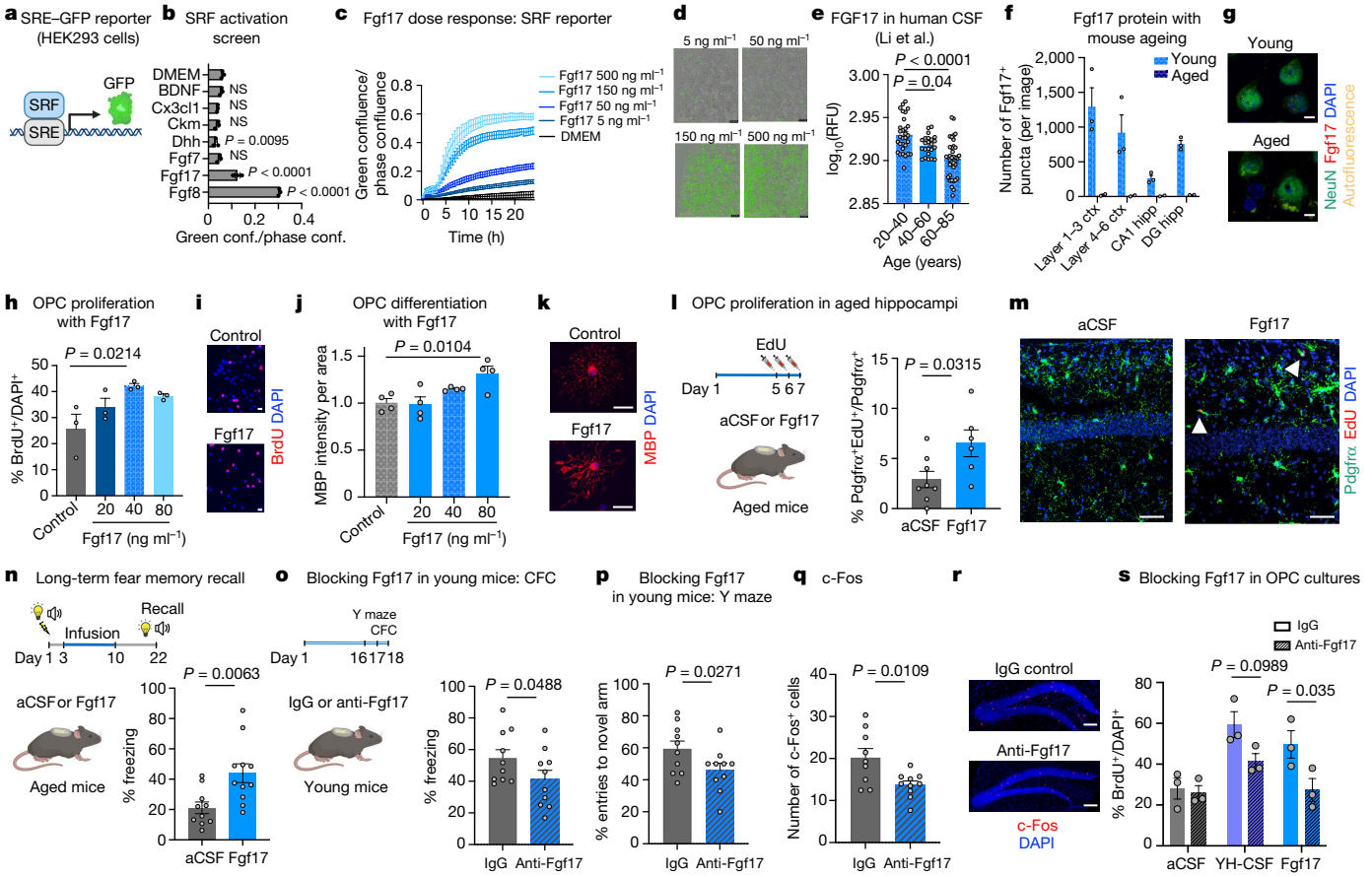

Fig. 4 | Fgf17 induces OPC proliferation and improves memory. a, Diagram of the SRE–GFP reporter in HEK293 cells. **b**, SRE–GFP activation by CSF ligands (500 ng ml^{-1}; $n = 3$; one-way ANOVA with Dunnett's multiple-comparisons test; mean ± s.e.m.). Conf., confluence; NS, not significant. **c**, Dose-dependent activation of the SRE–GFP reporter by Fgf17 ($n = 3$; one-way ANOVA with Tukey's post hoc test; mean ± s.e.m.). **d**, Representative images of the experiment in **c**. Scale bars, 400 µm. **e**, Meta-analysis of FGF17 levels in healthy human CSF[9] (ages 20–40 years, $n = 30$; ages 40–60 years, $n = 23$; ages 60–85 years, $n = 36$; one-way ANOVA with Dunnett's post hoc test; mean ± s.e.m.). RFU, relative fluorescence units. **f**, Number of Fgf17$^+$ puncta in the cortex and hippocampus of young (3 months) and aged (25 months) mice (young, $n = 3$; aged, $n = 2$; mean ± s.e.m.). Ctx, cortex; DG, dentate gyrus; Hipp, hippocampus. **g**, Representative images of the experiment in **f**. Scale bars, 5 µm. **h**, Percentage of proliferating OPCs treated with Fgf17 under proliferation conditions ($n = 3$; one-way ANOVA with Tukey's post hoc test; mean ± s.e.m.). **i**, Representative images of the experiment in **h**. Scale bars, 20 µm. **j**, MBP intensity per area in OPCs treated with Fgf17 under differentiation conditions (day 3) ($n = 4$; one-way ANOVA with Tukey's post hoc test; mean ± s.e.m.). **k**, Representative images of the experiment in **h**. Scale bars, 20 µm. **l**, Quantification of proliferating OPCs in the hippocampus of 20-month-old mice following 1 week of infusion with aCSF or Fgf17 (aCSF, $n = 8$; Fgf17, $n = 6$; two-sided t test; mean ± s.e.m.). **m**, Representative images of the experiment in **l**. Arrowheads point to proliferating OPCs. Scale bars, 50 µm. **n**, Percentage of freezing of 20-month-old mice in the remote recall contextual fear conditioning test (aCSF, $n = 10$; Fgf17, $n = 11$; two-sided t test; mean ± s.e.m.). **o**, Percentage of freezing of 3-month-old mice in the short-term contextual fear conditioning (CFC) test ($n = 10$; one-sided t test; mean ± s.e.m.). **p**, Percentage of entries to the novel arm of the forced-alternation Y maze ($n = 10$; one-sided t test; mean ± s.e.m.). **q**, Average number of active c-Fos$^+$ cells in the dentate gyrus (IgG, $n = 9$; anti-Fgf17, $n = 10$; two-sided t test; mean ± s.e.m.). **r**, Representative images of the experiment in **q**. Scale bars, 100 µm. **s**, Percentage of proliferating OPCs treated with aCSF, YH-CSF or Fgf17 in combination with IgG or anti-Fgf17 antibodies ($n = 3$; two-way ANOVA with Sidak's post hoc test; mean ± s.e.m.).

in other published human and mouse datasets of OPCs with age and Alzheimer's disease (AD) (Fig. 3g). Notably, *Srf* mRNA levels in neurons decreased with ageing and were not changed following acute injection with CSF (Extended Data Fig. 8e–h). Altogether, these experiments indicate that SRF signalling in OPCs is downregulated with ageing and induced following acute injection of young CSF in vivo.

Fgf17 mimics the effects of CSF on OPCs and memory

CSF contains hundreds of proteins that could potentially induce SRF signalling. We noticed that several SRF target genes are also known upstream inducers of SRF itself, such as BDNF and insulin-like growth factor 1 (IGF-1)[29,30]. On the basis of this observation, we cross-referenced two published CSF proteomic datasets[9,31] with the list of TRANSFAC-predicted SRF targets and generated a list of 35 potential SRF inducers (Supplementary Table 7). To test the activity of these candidates, we transfected HEK293 cells with an SRE–GFP reporter and added proteins at different concentrations (Fig. 4a). Fibroblast growth factor 8 (Fgf8) and Fgf17 induced the strongest dose-dependent responses (Fig. 4b–d and Extended Data Fig. 9a, b). We chose to proceed with Fgf17 because it is a brain-enriched protein (Extended Data Fig. 11a) and its levels decrease with age in human CSF (Fig. 4e), in human plasma in males and females[32], and in mouse neurons (Fig. 4f, g and Extended Data Fig. 10b–i). To gain better mechanistic understanding, we enhanced or inhibited actin polymerization using jasplakinolide and latrunculin A, respectively, and found that Fgf17 activates SRF signalling through actin modulation (Extended Data Fig. 9d). This indicates, as previously described for other growth factors, that Fgf17 activates the SRF pathway through Rho GTPase activation and modulation of actin dynamics[33]. We next performed the reporter experiment in the

presence of blocking antibodies for Fgfr1, Fgfr2 or Fgfr3 and found that Fgf17 reporter activation was dependent on signalling through Fgfr3 (Extended Data Fig. 9e). Interestingly, while Fgfr3 is very highly expressed by astrocytes, we also detected a fraction of Fgfr3-positive hippocampal OPCs (Extended Data Fig. 9f).

When added to primary rat OPCs, Fgf17 (40 ng ml^{-1}) induced OPC proliferation (Fig. 4h, i) and differentiation (Fig. 4j, k). Prior work with cultured OPCs has suggested that Fgf17 slightly promotes proliferation, although it may inhibit OPC differentiation in some contexts[34]. To determine their in vivo activity, we infused recombinant Fgf8 and Fgf17 into aged mice over 7 d, similar to administration of CSF (Fig. 1). Fgf17 induced OPC proliferation in the aged hippocampus, but Fgf8 did not (Fig. 4l, m and Extended Data Fig. 9c). We next tested the effect of Fgf17 infusion on cognition and found that it improved long-term memory performance in the remote memory recall paradigm described in Fig. 1 (Fig. 4n). These experiments demonstrate that Fgf17 is sufficient to mimic the effects of young CSF on OPCs in the hippocampus and on memory consolidation in aged mice.

Lastly, we infused young mice with an anti-Fgf17 blocking antibody ICV to test whether Fgf17 is necessary for normal memory function. We found that mice infused with anti-Fgf17, but not with control antibody, showed impaired performance in two hippocampal-dependent cognitive tests (Y maze and contextual fear conditioning; Fig. 4o, p) and impaired neuronal plasticity as measured by lower c-Fos levels in dentate gyrus granule cells following behavioural tests (Fig. 4q, r). In OPC cultures, the same concentration of anti-Fgf17 antibody inhibited OPC proliferation induced by young CSF or Fgf17. This indicates that the boost in proliferation is in part mediated by Fgf17 (Fig. 4s). Taken together, these experiments provide a link between Fgf17 and cognitive function, in young and aged mice.

Discussion

In summary, we discovered that young CSF is sufficient to improve memory function in aged mice, which occurs along with an increase in OPC proliferation and hippocampal myelination. Fgf17, whose levels decrease with age in mouse neurons and in human CSF, is sufficient and necessary to improve cognition in aged mice and promotes OPC proliferation in vivo and in vitro, suggesting that it constitutes a major component of the rejuvenating effects of young CSF (Working model in Extended data Fig. 11g). Moreover, young CSF induces expression of the transcription factor SRF and its actin cytoskeleton target genes to promote OPC proliferation. SRF is a versatile regulator of neuronal development and activity-dependent plasticity[24,35,36]. Here we find that it is also widely expressed by OPCs, where it is downregulated with ageing. It is interesting to speculate that SRF orchestrates plasticity in various cell types and that its loss with ageing promotes neurodegeneration. Expanding our examination of CSF proteins and SRF signalling in oligodendrocytes with ageing to other cell types could illuminate complex regulatory interactions within parenchymal cells and with the environment during development, ageing and ageing-related diseases.

The CSF proteome consists of proteins secreted by the choroid plexus or transferred through it from the blood plasma, as well as proteins secreted from parenchymal and immune cells. Heterochronic CSF experiments with cortical explants first demonstrated that developmental stage-specific CSF composition is critical for proper stem cell proliferation and brain development[4]. During ageing, improper signalling cues derived from the ageing choroid plexus were shown to lead to neuronal stem cell quiescence[5]. However, OPCs, which account for the largest population of stem cells in the aged brain, were mostly overlooked. Emerging studies in young rodents are revealing that oligodendrogenesis, the formation of myelinating oligodendrocytes from OPCs, is essential for consolidation of newly formed memories, implicating an active role for these cells in cognitive function[37–39]. A recent study showed that hippocampal oligodendrogenesis is markedly reduced with age and that increasing it was sufficient to improve performance in learning and memory tasks in aged mice[40] and in AD mouse models[41]. This is in line with studies showing that aged OPCs in white matter regions are slow to proliferate and to differentiate following demyelination in diseases such as multiple sclerosis and that local or systemic environmental manipulations restored their myelination capacity[42,43]. It is possible that these systemic therapeutic strategies affect OPCs through changes in CSF composition. Furthermore, mature oligodendrocytes are critical for maintenance of axonal health and for regulation of neuronal function. We cannot exclude the possibility that CSF proteins directly affect mature oligodendrocyte function with beneficial outcomes on neuronal health and cognitive function. Myelin plasticity is emerging as an important mechanism in learning and memory[44], and the study of myelin dysfunction in ageing-related cognitive decline is gaining interest.

As a proof of concept, we infused Fgf17 into the CSF of aged mice and found that it partially mimicked the effects of young CSF on OPC proliferation and long-term memory recall. Conversely, blocking Fgf17 by infusing mice with an inhibitory antibody resulted in impaired function in hippocampal-dependent memory tests. Fgf17 is critical for embryonic brain development[45], but not much is known about its function in the adult nervous system. We found that in the young adult mouse Fgf17 is abundantly expressed by cortical neurons and its expression drops markedly with ageing. Fgfr signalling is critical for oligodendrocyte development[46], with complex and diverse functions in disease processes such as demyelination and remyelination in multiple sclerosis[34]. Specifically, studies using *Fgf3r*-null mice have shown a delay in the terminal differentiation of pro-oligodendrocytes[47], and transient expression of Fgfr3 in subventricular zone progenitors drives oligodendrogenesis and promotes remyelination following a demyelinating injury[48]. Interestingly, young mice lacking *Fgf17* have smaller brains[49] and an array of social behaviour abnormalities coinciding with lower numbers of *Fos*-expressing cells in the prefrontal cortex following a novel social interaction test[50]. Further research is needed to demonstrate whether SRF, which regulates *Fos* expression, is involved in these circuits and potentially in neurodevelopmental and neuropsychiatric disorders. This strengthens the notion that studying CSF, the medium that has adapted to the unique needs of the brain, holds the potential to expand understanding of the brain's intricate mechanisms and cellular interactions.

Combined, our results suggest that targeting hippocampal myelination through factors present in young CSF might be a therapeutic strategy to prevent or rescue cognitive decline associated with ageing and neurodegenerative diseases.

Online content

Any methods, additional references, Nature Research reporting summaries, source data, extended data, supplementary information, acknowledgements, peer review information; details of author contributions and competing interests; and statements of data and code availability are available at https://doi.org/10.1038/s41586-022-04722-0.

1. Pluvinage, J. V. & Wyss-Coray, T. Systemic factors as mediators of brain homeostasis, ageing and neurodegeneration. *Nat. Rev. Neurosci.* **21**, 93–102 (2020).
2. Castellano, J. M. et al. Human umbilical cord plasma proteins revitalize hippocampal function in aged mice. *Nature* **544**, 488–492 (2017).
3. Villeda, S. A. et al. Young blood reverses age-related impairments in cognitive function and synaptic plasticity in mice. *Nat. Med.* **20**, 659–663 (2014).
4. Lehtinen, M. K. et al. The cerebrospinal fluid provides a proliferative niche for neural progenitor cells. *Neuron* **69**, 893–905 (2011).
5. Silva-Vargas, V., Maldonado-Soto, A. R., Mizrak, D., Codega, P. & Doetsch, F. Age-dependent niche signals from the choroid plexus regulate adult neural stem cells. *Cell Stem Cell* **19**, 643–652 (2016).
6. Fame, R. M. & Lehtinen, M. K. Emergence and developmental roles of the cerebrospinal fluid system. *Dev. Cell* **52**, 261–275 (2020).
7. Chen, C. P., Chen, R. L. & Preston, J. E. The influence of ageing in the cerebrospinal fluid concentrations of proteins that are derived from the choroid plexus, brain, and plasma. *Exp. Gerontol.* **47**, 323–328 (2012).

8. Baird, G. S. et al. Age-dependent changes in the cerebrospinal fluid proteome by slow off-rate modified aptamer array. *Am. J. Pathol.* **180**, 446–456 (2012).
9. Li, G. et al. Cerebrospinal fluid concentration of brain-derived neurotrophic factor and cognitive function in non-demented subjects. *PLoS ONE* **4**, e5424 (2009).
10. Pan, S., Mayoral, S. R., Choi, H. S., Chan, J. R. & Kheirbek, M. A. Preservation of a remote fear memory requires new myelin formation. *Nat. Neurosci.* **23**, 487–499 (2020).
11. Vetere, G. et al. Chemogenetic interrogation of a brain-wide fear memory network in mice. *Neuron* **94**, 363–374 (2017).
12. Fogel, S. M. et al. fMRI and sleep correlates of the age-related impairment in motor memory consolidation. *Hum. Brain Mapp.* **35**, 3625–3645 (2014).
13. Gibson, E. M. et al. Neuronal activity promotes oligodendrogenesis and adaptive myelination in the mammalian brain. *Science* **344**, 1252304 (2014).
14. Dugas, J. C. & Emery, B. Purification of oligodendrocyte precursor cells from rat cortices by immunopanning. *Cold Spring Harb. Protoc.* **2013**, 745–758 (2013).
15. Sun, L. O. et al. Spatiotemporal control of CNS myelination by oligodendrocyte programmed cell death through the TFEB–PUMA axis. *Cell* **175**, 1811–1826 (2018).
16. Zuchero, J. B. et al. CNS myelin wrapping is driven by actin disassembly. *Dev. Cell* **34**, 152–167 (2015).
17. Schwarz, N. et al. Human cerebrospinal fluid promotes long-term neuronal viability and network function in human neocortical organotypic brain slice cultures. *Sci. Rep.* **7**, 12249 (2017).
18. Wentling, M. et al. A metabolic perspective on CSF-mediated neurodegeneration in multiple sclerosis. *Brain* **142**, 2756–2774 (2019).
19. Mathur, D. et al. Bioenergetic failure in rat oligodendrocyte progenitor cells treated with cerebrospinal fluid derived from multiple sclerosis patients. *Front. Cell. Neurosci.* **11**, 209 (2017).
20. Braun, T. & Gautel, M. Transcriptional mechanisms regulating skeletal muscle differentiation, growth and homeostasis. *Nat. Rev. Mol. Cell Biol.* **12**, 349–361 (2011).
21. Guo, Y. et al. Hierarchical and stage-specific regulation of murine cardiomyocyte maturation by serum response factor. *Nat. Commun.* **9**, 3837 (2018).
22. Knoll, B. & Nordheim, A. Functional versatility of transcription factors in the nervous system: the SRF paradigm. *Trends Neurosci.* **32**, 432–442 (2009).
23. Miralles, F., Posern, G., Zaromytidou, A. I. & Treisman, R. Actin dynamics control SRF activity by regulation of its coactivator MAL. *Cell* **113**, 329–342 (2003).
24. Knoll, B. et al. Serum response factor controls neuronal circuit assembly in the hippocampus. *Nat. Neurosci.* **9**, 195–204 (2006).
25. Lahoute, C. et al. Premature aging in skeletal muscle lacking serum response factor. *PLoS ONE* **3**, e3910 (2008).
26. Mergoud Dit Lamarche, A. et al. UNC-120/SRF independently controls muscle aging and lifespan in *Caenorhabditis elegans*. *Aging Cell* **17**, e12713 (2018).
27. Ximerakis, M. et al. Single-cell transcriptomic profiling of the aging mouse brain. *Nat. Neurosci.* **22**, 1696–1708 (2019).
28. Falcao, A. M. et al. Disease-specific oligodendrocyte lineage cells arise in multiple sclerosis. *Nat. Med.* **24**, 1837–1844 (2018).
29. Iacono, G., Altafini, C. & Torre, V. Early phase of plasticity-related gene regulation and SRF dependent transcription in the hippocampus. *PLoS ONE* **8**, e68078 (2013).
30. Kuzniewska, B. et al. Brain-derived neurotrophic factor induces matrix metalloproteinase 9 expression in neurons via the serum response factor/c-Fos pathway. *Mol. Cell. Biol.* **33**, 2149–2162 (2013).
31. Sasayama, D. et al. Genome-wide quantitative trait loci mapping of the human cerebrospinal fluid proteome. *Hum. Mol. Genet.* **26**, 44–51 (2017).
32. Sathyan, S. et al. Plasma proteomic profile of age, health span, and all-cause mortality in older adults. *Aging Cell* **19**, e13250 (2020).
33. Esnault, C. et al. Rho–actin signaling to the MRTF coactivators dominates the immediate transcriptional response to serum in fibroblasts. *Genes Dev.* **28**, 943–958 (2014).
34. Fortin, D., Rom, E., Sun, H., Yayon, A. & Bansal, R. Distinct fibroblast growth factor (FGF)/FGF receptor signaling pairs initiate diverse cellular responses in the oligodendrocyte lineage. *J. Neurosci.* **25**, 7470–7479 (2005).
35. Ramanan, N. et al. SRF mediates activity-induced gene expression and synaptic plasticity but not neuronal viability. *Nat. Neurosci.* **8**, 759–767 (2005).
36. Etkin, A. et al. A role in learning for SRF: deletion in the adult forebrain disrupts LTD and the formation of an immediate memory of a novel context. *Neuron* **50**, 127–143 (2006).
37. Pan, S., Mayoral, S. R., Choi, H. S., Chan, J. R. & Kheirbek, M. A. Preservation of a remote fear memory requires new myelin formation. *Nat. Neurosci.* **23**, 487–499 (2020).
38. Xiao, L. et al. Rapid production of new oligodendrocytes is required in the earliest stages of motor-skill learning. *Nat. Neurosci.* **19**, 1210–1217 (2016).
39. Steadman, P. E. et al. Disruption of oligodendrogenesis impairs memory consolidation in adult mice. *Neuron* **105**, 150–164 (2020).
40. Wang, F. et al. Myelin degeneration and diminished myelin renewal contribute to age-related deficits in memory. *Nat. Neurosci.* **23**, 481–486 (2020).
41. Chen, J. F. et al. Enhancing myelin renewal reverses cognitive dysfunction in a murine model of Alzheimer's disease. *Neuron* **109**, 2292–2307 (2021).
42. Segel, M. et al. Niche stiffness underlies the ageing of central nervous system progenitor cells. *Nature* **573**, 130–134 (2019).
43. Neumann, B. et al. Metformin restores CNS remyelination capacity by rejuvenating aged stem cells. *Cell Stem Cell* **25**, 473–485 (2019).
44. Bonetto, G., Belin, D. & Karadottir, R. T. Myelin: a gatekeeper of activity-dependent circuit plasticity? *Science* **374**, eaba6905 (2021).
45. Xu, J., Liu, Z. & Ornitz, D. M. Temporal and spatial gradients of Fgf8 and Fgf17 regulate proliferation and differentiation of midline cerebellar structures. *Development* **127**, 1833–1843 (2000).
46. Furusho, M., Ishii, A., Hebert, J. M. & Bansal, R. Developmental stage-specific role of Frs adapters as mediators of FGF receptor signaling in the oligodendrocyte lineage cells. *Glia* **68**, 617–630 (2020).
47. Oh, L. Y. et al. Fibroblast growth factor receptor 3 signaling regulates the onset of oligodendrocyte terminal differentiation. *J. Neurosci.* **23**, 883–894 (2003).
48. Kang, W., Nguyen, K. C. Q. & Hebert, J. M. Transient redirection of SVZ stem cells to oligodendrogenesis by FGFR3 activation promotes remyelination. *Stem Cell Rep.* **12**, 1223–1231 (2019).
49. Jen, Y. H., Musacchio, M. & Lander, A. D. Glypican-1 controls brain size through regulation of fibroblast growth factor signaling in early neurogenesis. *Neural Dev.* **4**, 33 (2009).
50. Scearce-Levie, K. et al. Abnormal social behaviors in mice lacking Fgf17. *Genes Brain Behav.* **7**, 344–354 (2008).

Methods

Animals

Aged C57BL/6 mice (18–22 months old) were obtained from the National Institute on Aging rodent colony. Young male C57BL/6 mice (2 months old) were obtained from Charles River Laboratories or Jackson Laboratories. All experiments used male mice. All mice were housed at the Palo Alto VA animal facility under a 12-h light/12-h dark cycle with dark hours from 18:30–06:30 and housed at 68–73 °F under 40–60% humidity. We used published data[2,3,51] to determine an optimal *n* for our studies on the effects of young CSF on behaviour. For bulk RNA-seq of sorted oligodendrocyte nuclei, we performed preliminary studies to ensure that we would capture enough nuclei for downstream library preparation and statistical analysis. Age-matched mice were allocated into groups to achieve an equal average weight. All other criteria were not considered and, as such, were randomized. All animal care and procedures complied with the Animal Welfare Act and were in accordance with institutional guidelines and approved by the VA Palo Alto Committee on Animal Research and the institutional administrative panel of laboratory animal care at Stanford University.

YM-CSF collection

CSF was collected as previously described with several adaptations[52]. In brief, 10-week-old mice were anaesthetized intraperitoneally with ketamine (120 mg kg^{-1}) and xylazine (8 mg kg^{-1}) and then placed in a stereotactic instrument (KOPF) with the head secured at a 45-degree angle facing downwards. An incision was made above the neck and the muscles were held separated with microretractors, allowing exposure of the cisterna magna by blunt forceps without any bleeding. CSF was pulled out of the cisterna magna cavity with a 20-µl pipettor connected through an aspirator tube assembly (Sigma, A5177) to a pulled glass capillary (borosilicate glass tubes; internal diameter, 1.30 mm; outer diameter, 1.70 mm; length, 4.00 in; type 8250, King Precision Glass) held secure by a model 1769 90° electrode holder (KOPF). CSF was kept in a low-protein bind tube on ice and spun in a cold centrifuge for 10 min at 1,500 r.p.m. to exclude CSF immune cells. Supernatant was collected and kept at −80 °C until use. The pellet was resuspended in 6 µl of milli-Q ultra-pure water for blood contamination quality control using the Nanodrop UV–visible light setting with a 415-nm wavelength for detection of oxyhaemoglobin[53]. A cut-off of below 0.02 AU was used for CSF infusions.

Human CSF

CSF samples from nine young heathy individuals (ages 24–26 years) were obtained through a collaboration with H.Z. (University of Gothenburg, Sweden). The study was approved by the regional ethics committee at the University of Gothenburg, and informed consent was obtained from all participants[54,55]. The samples were baseline (normal sleep) lumbar CSF samples, collected in the morning, from healthy volunteers who took part in a study on sleep restriction-induced changes in CSF composition. For in vitro experiments, three pools each consisting of samples from three individuals were made for each experiment; two pools from six male samples and one pool from female samples were each used in 3–4 technical triplicates. AH-CSF from healthy individuals (ages 65–76 years) was obtained from the Stanford Alzheimer's Disease Research Center.

Osmotic pump ICV infusion

To minimize the volume of mouse CSF infused per mouse, young CSF or aCSF was loaded into a coiled polyethylene (PE-60) catheter prepared in house following the lynch coil technique[56]. In brief, the total length of the coil needed was calculated by assuming an internal volume of 4.56 µl for each centimetre of tube. Typically, 20 cm was wound around a syringe of the same outside diameter as the pump and secured with tape. The syringe was submerged in boiling water for 1 min and immediately immersed in ice-cold water for 1 min. Coils were disassembled and left to dry overnight. Then, 90 µl of pooled young CSF or aCSF (Tocris) was loaded into the coiled catheter connected to a 100-µl osmotic pump (Alzet, 1007D) with a 7-d infusion at a rate of 0.5 µl h^{-1}. Osmotic pumps were connected to a cannula (Brain Infusion Kit III, Alzet) and incubated overnight in a 37 °C water bath. The cannula was inserted at +1 mm medio-lateral, 0 mm anterior–posterior and −3 mm dorso-ventral relative to the bregma to target the right lateral ventricle. The pump was placed subcutaneously, and mice received postsurgical buprenorphine and Baytril. In the human CSF infusion experiments, a pool of three young or three aged human CSF samples, pooled YM-CSF or aCSF was loaded into an osmotic pump (without a coil) and surgery was performed as described above. Recombinant carrier-free human/mouse Fgf8b (423-F8/CF, R&D) and mouse Fgf17 (7400-FG-025/CF, R&D) were resuspended in aCSF (Tocris) to a concentration of 25 µg ml^{-1} and loaded into an osmotic pump (Alzet, 1007D) with 7-d infusion at a rate of 0.5 µl h^{-1}. In experiments with anti-Fgf17 blocking antibody, polyclonal rabbit anti-Fgf17 (PA5-109722, Thermo) and a rabbit IgG isotype control (31235, Thermo) were diluted in aCSF, loaded on a 3-kDa MWCO Amicon Ultra centrifugal filter (UFC500396, ThermoFisher) for buffer exchange and spun at 14,000*g* for 30 min at 4 °C. This step was repeated twice. Osmotic pumps (Alzet, 1004) were loaded with 0.68 mg ml^{-1} antibody to achieve a final CSF steady-state concentration of 5 µg ml^{-1}. Surgery was performed as described above. In all experiments, mice were split into groups to achieve an equal average body weight in all groups.

Acute ICV injection

Eighteen-month-old mice were anaesthetized with 2.5% isoflurane and then placed in a stereotactic instrument (KOPF). Then, 3 µl of a pool of YM-CSF (as described above) or aCSF was injected into the right lateral ventricle using a digital pump (WPI syringe pump with Micro4t controller model UMP3T-1) at a rate of 1 µl min^{-1}. At 1 or 6 h following the injection, mice were perfused and the contralateral hippocampus was dissected and used for RNA-seq to avoid gene signatures induced by local immune response to the surgery. In labelled Fgf17 experiments, 10 µg of mouse Fgf17 (7400-FG-025/CF, R&D) was conjugated to Alexa Fluor 647 using the lightning-link conjugation kit (ab269823, ThermoFisher) following the manufacturer's instructions and then loaded twice on a 3-kDa MWCO Amicon Ultra centrifugal filter (UFC500396, ThermoFisher) and spun at 14,000*g* for 30 min at 4 °C for free-dye clean-up and buffer exchange with aCSF. As control, a parallel labelling reaction (dye-only control) was carried out with a similar volume of aCSF as input. In CSF labelling experiments, 1 ml of human CSF was conjugated to Alexa Fluor 647 (ThermoFisher) using NHS chemistry and then loaded on a 3-kDa MWCO Amicon Ultra centrifugal filter (UFC500396, ThermoFisher) and spun at 14,000*g* for 30 min at 4 °C for free-dye clean-up and buffer exchange with aCSF and for protein concentration. Then, 0.5 µg of labelled Fgf17 in 2 µl, dye-only control or YH-CSF was injected at a rate of 1 µl min^{-1} into young (2–3 months) mice and mice were killed 2 or 3 h after injection. Mice received postsurgical buprenorphine and Baytril.

Behavioural assays

In the remote fear conditioning recall test, mice were trained to associate cage context or an audiovisual cue with an aversive stimulus (foot shock). On day 1, mice were placed in a cage and exposed to three periods of 30 s of paired cue light and 1,000-Hz tone followed by a 2-s foot shock (0.6 mA), with a 60-s interval. On day 2 and day 22, mice were subjected to two trials. In the first trial assessing contextual memory, mice were re-exposed to the same cage context and freezing behaviour was measured for 390 s using a FreezeScan tracking system (Cleversys). In the second trial measuring cued memory, mice were placed in a novel context and exposed to the same cue light and tone from day 1 on minutes 2, 3 and 4 of the trial. Freezing behaviour was averaged across

minutes 3–5. No significant differences in contextual fear conditioning were observed between groups at day 22. All experiments were performed by a blinded researcher. In the experiment presented in Fig. 1b, initial group numbers were $n = 11$ for aCSF and $n = 9$ for YM-CSF (owing to limited amounts of mouse CSF) and one mouse from each group died during the experiment. In the experiment presented in Fig. 4n, initial group numbers were $n = 11$ for aCSF (this was supposed to be $n = 12$, but one pump was not implanted owing to an air bubble) and $n = 12$ for Fgf17 and one mouse from each group died during the experiment.

In the anti-Fgf17 blocking antibody experiments, the forced-alternation Y-maze and contextual fear conditioning tests were performed as previously described[57]. The forced-alteration Y-maze test consisted of a 5-min training trial followed by a 5-min retrieval trail, with a 1-h intertrial interval. For the training trial, one arm of the Y maze was blocked off and mice were allowed to explore the two open arms. One hour later, the mouse was again placed in the Y maze with all three arms open and a black-and-white pattern placed at the end of the novel arm. Between mice and trials, the maze was wiped with ethanol to remove odour cues. For analysis, video was analysed by a blinded observer and both the number of arm entries and the time spent in each arm were quantified. In the fear conditioning paradigm, mice were trained to associate cage context or an audiovisual cue with an aversive stimulus (foot shock). The test was administered over 2 d. On day 1, mice were placed in a cage and exposed to two periods of 30 s of paired cue light and 1,000-Hz tone followed by a 2-s foot shock (0.6 mA), with a 180-s interval. On day 2, mice were subjected to two trials. In the first trial assessing contextual memory, mice were re-exposed to the same cage context and freezing behaviour was measured during minutes 1–3 using a FreezeScan tracking system (Cleversys). In the second trial measuring cued memory, mice were placed in a novel context and exposed to the same cue light and tone from day 1 after 2 min of exploration. Freezing behaviour was measured for 1–3 min following the cue. No significant differences in cued fear conditioning were observed between groups. Experimental groups consisted of $n = 10$ mice, and no mice were excluded during the experiment.

In vivo BrdU and EdU pulses

To assess baseline proliferation, mice received one EdU injection 15 min before the stereotactic surgery (Invitrogen, E10415; 100 mg kg^{-1} intraperitoneally). To assess cell proliferation after infusion, mice were pulsed three times with BrdU to label proliferating cells: twice on day 5 of the infusion 10 h apart and once on day 6 at 2 h before perfusion (100 mg kg^{-1} intraperitoneally; B5002-5G, Sigma-Aldrich). In all subsequent cohorts, mice received postinfusion pulses of EdU instead of BrdU in the same paradigm described above, with no baseline labelling before surgery.

Tissue processing before immunostaining

Mice were anaesthetized with Avertin (2,2,2-tribromoethanol: T48402, Sigma-Aldrich; 2-methyl-2-butanol: 240486, Sigma-Aldrich) (0.018 ml (2.5%) per gram of body weight) and perfused with 20 ml cold PBS. Brains were collected and divided sagittally. One hemisphere was used to dissect the hippocampus for RNA-seq and was snap frozen and stored at −80 °C. The second hemisphere was fixed in phosphate-buffered 4% paraformaldehyde (PFA) overnight at 4 °C before transfer to 30% sucrose in PBS at 4 °C until sectioning. Brains were frozen at −30 °C and cryosectioned coronally at 40 µm with a microtome (Leica, SM2010R). Brain sections were stored in cryoprotectant (40% PBS, 30% glycerol, 30% ethylene glycol) and kept at −20 °C until staining.

Immunostaining

Immunofluorescence staining of brain slices. Brain sections were washed three times for 10 min each in TBST and then blocked in TBS++ (TBS + 3% donkey serum (130787, Jackson ImmunoResearch) + 0.25% Triton X-100 (T8787, Sigma-Aldrich)) for 1 h, followed by incubation with primary antibody overnight on a rocking platform at 4 °C. The following primary antibodies were used in this study: PDGF receptor α (D1E1E) XP rabbit mAb (1:500; Cell Signaling, 3174), rabbit anti-MBP (1:100; Millipore, MAB386), rabbit anti-Fgf17 (1:500; Thermo, PA5-109722), rabbit anti-c-Fos (1:500; Cell Signaling, 9F6), rabbit anti-GFAP (1:500; Dako, Z0334), goat anti-IBA1 (1:500; Abcam, ab5076), rabbit anti-NG2-Alexa488 (1:200; Millipore, AB5230A4), rabbit anti-Olig2 (1:500; Millipore, AB9610), anti-Acta2-Cy3 (1:500; Sigma, C6198) and mouse anti-NeuN (1:500; Sigma, MAB377). For secondary staining, brain sections were washed three times for 10 min each in TBST, followed by incubation for 1.5 h with Alexa Fluor-conjugated secondary antibodies (1:500). For in vivo phalloidin staining, phallidin-Alexa488 (ref. [58]; Thermo, A12379) was added at a 1:50 dilution to the secondary antibody mix. Brain sections were washed and mounted on SuperFrost microscope slides (Fisher Scientific, 12-550-15) with Vectashield Hardset Antifade Mounting Medium with DAPI (Vector Labs, H-1500/NC9029229). For MBP staining, an additional step of tissue delipidation was performed before blocking: tissues were incubated in 100% ethanol for 10 min at room temperature and then washed twice with PBS.

EdU staining. Brain sections were washed three times for 10 min each in PBS and then permeabilized for 20 min in 0.1% Triton X-100 (Sigma-Aldrich, T8787), washed again three times and then blocked in TBS++ for 1 h. EdU staining was performed following the instructions for the Click-iT Plus EdU Alexa Fluor 555 Imaging Kit (Life Technologies, C10638). Sections were washed and stained with primary and secondary antibodies as described above.

BrdU staining: brain slices and 384-well plates. Following staining with other primary and secondary antibodies, sections were incubated in 2 N HCl for 30 min at 37 °C and then washed three times for 10 min each in TBST. Sections were blocked for 1.5 h in TBS++ and then transferred to primary antibody mix with rat anti-BrdU antibody (1:500; Abcam, ab6326) overnight at 4 °C. Secondary staining started with three washes for 10 min each in TBST, followed by incubation with secondary antibody mix for 1.5 h. After three 10-min washes in TBST, sections were mounted as described above. For 384-well plates, nuclei were stained with Hoechst 33342 (1:2,000; Thermo, H3570) and immediately imaged on a Keyence microscope (BZ-X800). In cases where BrdU and EdU staining were performed on the same sections, the sequence was as follows: permeabilization, HCl antigen retrieval, EdU Click-iT reaction, blocking, and primary and secondary antibody staining as described above in detail.

In situ RNA hybridization (RNAscope)

RNAscope was performed on fresh frozen coronal brain sections (10 µm thick) using the Multiplex Fluorescence v.2 kit (Advanced Cell Diagnostics) according to the manufacturer's protocol with minor modifications. Tissue fixation with 4% PFA was extended to 60 min at room temperature, and protease IV treatment was shortened to 20 min to better preserve the hippocampal tissue. Probes for mouse *Pdgfra*, *Srf*, *Fgfr3* and *Fgf17* were commercially available from the manufacturer, and secondary Opal 690 and 520 reagents (FP1497001KT and FP1487001KT, Akoya Biosciences) were diluted 1:1,500 in TSA buffer.

Image analysis (Imaris)

Brain slices. Confocal *z* stacks of four coronal brain sections spanning the dorsal hippocampus were captured on a Zeiss confocal LSM880 microscope for each brain sample using ×20 magnification. Maximum-projection files (at least four hippocampal coronal slices per mouse, 400 µm apart) were analysed in Imaris by generating masks of two main regions of interest: (1) CA1: stratum oriens, stratum pyramidale and stratum lacunosum-moleculare (SLM) combined and (2) cortex. The percentage of newly proliferated OPCs was analysed by dividing the cell count for $BrdU^+$Pdgfrα+or EdU^+Pdgfrα+ cells by that

for Pdgfrα$^+$ cells. For cell density, the BrdU$^+$ or Pdgfrα$^+$ cell count was divided by the corresponding area of the mask per slice.

For RNAscope analysis, similar hippocampal tiled *z* stacks were acquired (at least four hippocampal coronal slices per mouse, 100 µm apart). The percentage of *Srf*$^+$ OPCs was calculated by dividing the number of *Srf*$^+$Pdgfra$^+$ nuclei by the number of Pdgfra$^+$ nuclei in the CA1 region of the hippocampus. For MBP analysis, confocal images of the molecular layer were acquired using ×20 magnification. MBP intensity was measured using batch analysis in ImageJ. For in vivo phalloidin analysis, *z* stacks at ×63 magnification of individual OPCs were obtained by staining for Pdgfrα. Using Imaris, three-dimensional surface rendering was reconstructed by Pdgfrα signal and phalloidin intensity was measured only inside the surface. All analyses were performed by a blinded observer.

In vitro cell culture. Three random ×20 images of each well were analysed using Imaris batch by setting similar surfaces to automatically count BrdU$^+$ and Hoechst$^+$ nuclei. For each image, the percentage of proliferating cells was calculated by dividing the number of BrdU$^+$ cells by the total number of Hoechst$^+$ cells. In differentiation experiments, cell morphology state was assessed manually as previously described[16]. Cellular phalloidin intensity and MBP intensity were measured by manually delineating cell borders and measuring intensity and cell area; all cell measurements were then averaged per coverslip. Representative images of phalloidin intensity were generated with Fire LUT in ImageJ. All other quantifications were performed using ImageJ and manual cell counts. All analyses were performed by a blinded observer.

Transmission electron microscopy

Perfusion and sectioning. Mice were perfused with 20 ml cold EM fixation buffer consisting of EM-grade 2% glutaraldehyde (EMS/Fisher, 50-262-08) and 4% PFA (EMS/Fisher, 50-980-486) in 0.2 M sodium cacodylate (EMS/Fisher, 50-980-279) and kept in fixation buffer until sectioning. Brains were sectioned coronally to 100-µm sections using a Leica VT1200S vibratome and kept in EM fixative until TEM processing.

High-pressure freezing with freeze substitution. Vibratome sections of 100 µm were stained using an osmium–thiocarbohydrazide–osmium (OTO) method[59,60] in combination with microwave-assisted processing, followed by high-pressure freezing and freeze substitution (HPF–FS), as previously described[61]. In brief, samples were stained with OTO, incubated with 2% aqueous uranyl acetate overnight and then subjected to HPF, followed by super-rapid FS[62] with 4% osmium tetroxide, 0.1% uranyl acetate and 5% ddH_2O in acetone; they were then thin-layer embedded and polymerized in hard epon resin. Resin-embedded samples were precision cut off the glass slide and glued with cyanoacrylate onto a blank resin block for sectioning or glued with silver paint onto a stub for focused ion beam imaging.

Transmission electron microscopy. Ultrathin sections of 90 nm were cut using a Leica UC6 ultramicrotome (Leica Microsystems) and collected onto formvar-coated 50-mesh copper grids or copper–rhodium slot grids. Because of native contrast from volume EM processing, no poststain was necessary. Sections were imaged using a Tecnai 12 120-kV transmission electron microscope (FEI), data were recorded using an UltraScan 1000 with Digital Micrograph 3 software (Gatan) and SerialEM was used to collect montages covering an area of 143 x 143 µm.

SRF reporter assays

HEK293 cells (ATCC) were plated at 50,000 cells per well in a 96-well plate in full medium (DMEM with 10% FCS and 1% penicillin-streptomycin) and transfected on day 2 with the Cignal SRE Reporter Assay Kit (GFP) (Qiagen, CCS-010G) using Lipofectamine P3000 in experimental medium (DMEM with 0.5% FCS and 1% non-essential amino acids (Sigma, M7145)), following the manufacturer's instructions. On day 3, the medium was changed to 90 µl fresh experimental medium and supplemented with 10 µl of a 10× solution of carrier-free recombinant human KGF/FGF-7 (R&D, 251-KG-010), human/mouse Fgf8b (R&D, 423-F8/CF), mouse Fgf17 (R&D, 7400-FG-025/CF), human/murine/rat BDNF (Peprotech, 450-02), human CX3CL1/fractalkine (R&D, 365-FR-025), human Dhh (Abcam, ab78682) or Ckm (R&D, 9070-CK-050) at the indicated concentration. Plates were incubated in an IncuCyte (Essen BioScience) and imaged every hour for 24 h. In actin inhibitor experiments, on day 3, the medium was changed to fresh experimental medium and cells were pre-incubated for 30 min at 37 °C with jasplakinolide (125 or 250 nM; Fisher Scientific, J7473) or latrunculin A (250 or 500 nM; Thermo, L12370), before adding Fgf17 at a final concentration of 200 ng ml^{-1}. Plates were incubated in the IncuCyte and imaged every hour for 24 h. In anti-FgfR blocking antibody experiments, on day 3, the medium was changed to fresh experimental medium and cells were pre-incubated at 37 °C with anti-FgfR1 (NBP2-12308), anti-FGFR2 (MAB684-100) or anti-FGFR3 (MAB7661-100; all from Novus Biologicals) at a final concentration of 50 µg ml^{-1}, before adding Fgf17 at a final concentration of 200 ng ml^{-1}. Plates were incubated in the IncuCyte and imaged every hour for 24 h. HEK293 cells were not authenticated and were not tested for mycoplasma contamination.

OPC primary cultures

Rat OPC cultures. OPCs were isolated from postnatal day 7 (P7)–P8 Sprague–Dawley (Charles River) rat brains by immunopanning and grown in serum-free defined medium, as previously described[63]. Cell culture for proliferation and differentiation experiments was performed following the protocol with several modifications. To use the least possible amount of CSF from young healthy humans, we minimized the culture conditions to 384-well plates. In addition, to account for inter-participant variability, we pooled CSF from three individuals with similar ages and used three such pools in each experiment in triplicate. Following initial growth for 4 d in 10-cm dishes, cells were trypsinized and split into 384-well plates (Falcon 384-Well Optilux, 353962) coated with poly(D-lysine) (Sigma-Aldrich, P6407; molecular weight, 70–150 kDa). For proliferation experiments, 2,500 cells were plated in a total volume of 50 µl of full proliferation medium supplemented with 10 ng ml^{-1} PDGF (Peprotech, 100-13A), 10 ng ml^{-1} CNTF (Peprotech, 450-02), 4.2 µg ml^{-1} forskolin (Sigma-Aldrich, F6886) and 1 ng ml^{-1} NT3 (Peprotech, 450-03) along with 10% YH-CSF or aCSF. Actin filaments were visualized by live imaging with the addition of 500 nM SiR-actin (Cytoskeleton, CY-SC002) along with 10% YH-CSF. Wells were imaged every hour for the remaining 6 h of the experiment. In BrdU experiments, 18 h after plating in 384-well plates (with 10% CSF), 5 µl of 200 µM BrdU (20 µM final concentration) was added for a pulse of 6 h followed by fixation with 4% PFA for 20 min. BrdU experiments were performed with the indicated concentrations of YH-CSF or Fgf17 and in Fig. 4s in combination with rabbit anti-Fgf17 (Thermo, PA5-109722) or IgG isotype control (Thermo, 31235) to achieve a final concentration of 5 µg ml^{-1} antibody, 40 ng ml^{-1} Fgf17 and 10% YH-CSF in full proliferation medium, as indicated above.

In experiments that required phalloidin staining, 10,000 OPCs were plated on poly(D-lysine)-covered 12-mm coverslips in a 24-well dish in 90% full proliferation medium (315 µl) and let to adhere overnight; the medium was then supplemented with 10% CSF (35 µl) for 6 h. Coverslips were fixed with 4% PFA for 20 min, washed and stained with 555-phalloidin in PBS (1:143; Invitrogen) for 15 min. Coverslips were washed and mounted with Vectashield Hardset Antifade Mounting Medium with DAPI (Vector Labs, H-1500/NC9029229). For differentiation experiments, 10,000 OPCs were plated on poly(D-lysine)-covered 12-mm coverslips in a 24-well dish in full proliferation medium overnight. Proliferation medium was changed completely to differentiation medium (basal growth medium supplemented with 40 ng ml^{-1} T_3 (Sigma-Aldrich, T6397)) with 10% CSF, with a 50% medium change (with 10% CSF) on day 2 of differentiation. At day 4 of differentiation,

coverslips were fixed with 4% PFA for 20 min, washed with PBS and permeabilized with 0.1% Triton X-100 for 3 min followed by washing and blocking in 3% BSA for 1 h. Primary antibodies used were as follows: rabbit anti-MBP (1:100; Abcam, ab7349; knockout validated[16]) and mouse anti-GFAP (1:500; Chemicon, MAB360). Primary antibodies were incubated with cells overnight at 4 °C. Coverslips were washed, stained with Alexa Fluor-conjugated secondary antibodies (1:500) followed by a 15-min stain with Cell Mask (1:1,000; Invitrogen, C10046), mounted and set on a slide before imaging on a Keyence microscope (BZ-X800) or confocal laser-scanning microscope (Zeiss LSM880).

Mouse OPC cultures. Mouse OPCs were purified from the brains of mice with *loxP*-flanked *Srf* (generated by D. Ginty and kindly provided by E. Small) by immunopanning as described above for rat OPCs[63].

On day 3 of culture, $Srf^{F/F}$ OPCs were split and plated in 384-well plates for proliferation experiments. When cells were in suspension in proliferation medium before plating, 1×10^{10} viral genomes of AAV DJ-CMV eGFP-deleted cre (GVVC-AAV-62) or AAV DJ-CMV eGFP-cre (GVVC-AAV-63) (both generated by the Stanford Gene Vector and Virus Core) were added. The following day, the medium was fully replaced, and 48 h after infection 10% aCSF or YH-CSF was added to the proliferation medium with BrdU (20 µM final concentration) for 16 h. Cells were fixed and cell proliferation was assessed as indicated above for BrdU experiments.

SLAMseq experiment and data analysis

The optimal s^4U concentration was assessed using the SLAMseq[64] Explorer Kit—Cell Viability Titration Module (Lexogen, 061) following the manufacturer's recommendations. In brief, OPCs were incubated with increasing doubling concentrations of s^4U (1.95–2,000 µM) and viability was assessed with ATP incorporation following the manufacturer's recommendations (Promega, G7571). A final concentration of 62.5 µM was found to be the highest concentration that did not compromise cell viability within 12 h (twice the duration of the intended experiment). The SLAMseq experiment was conducted following the protocol for the SLAMseq Kinetics Kit—Anabolic Kinetics Module (Lexogen, 061). In brief, following initial growth for 4 d in 10-cm dishes, 30,000 OPCs were plated in 315 µl full proliferation medium on poly(D-lysine)-covered 24-well plates (one plate per time point) overnight. The next day, 35 µl of pooled YH-CSF or aCSF spiked with 625 µM s^4U (10× concentration) was added gently to minimize confounding induction of gene expression. After 1 or 6 h, the medium was removed and cells were scraped with 1 ml TRIzol (Thermo, 15596018), transferred to foil-covered tubes and frozen until RNA extraction. RNA extraction was performed following the protocol for the anabolic kit. All cell culture and RNA extraction steps were performed in the dark under red light, following the manufacturer's recommendations. Library preparation was performed with the QuantSeq 3′ mRNA-Seq Library Prep Kit for Illumina (FWD) (Lexogen, 015) with the indicated modifications to adjust to low-RNA input. After normalization and pooling, libraries were sequenced on a NextSeq 550 (Illumina) using single-end 75-bp reads. Libraries were sequenced to a mean depth of ~30 million reads per sample. Raw sequencing files were demultiplexed with bcl2fastq, and resulting FASTQ files were combined across lanes and per sample. Sequencing quality control was performed using FastQC v0.11.8, and summary reports were generated with MultiQC v1.7. FASTQ files were then analysed using SLAM-DUNK pipeline v0.3.4 and the related alleyoop toolchain. The pipeline comprises (1) read mapping, (2) alignment filtering, (3) SNP calling and correction, and (4) 3′-UTR sequence counting. Using NextGenMap, reads were aligned against the genome of *Rattus norvegicus* (release 6.0), which was downloaded in FASTA format from Ensembl release v97. For mapping, the following parameters were set: '-5 12, -a 4, -n 1, -ss', with the rest left at default. Resulting BAM-format files were filtered to remove low-quality alignments using the parameters '-mq 2, -mi 0.95, -nm -1', with the rest left at default. Next, SNPs in alignments, in particular T>C conversions, were called with parameters '-c 10, -f 0.8' with the other parameters remaining at default. The statistical independence of distributions of true SNP calls identified by VarScan2 in relation to the number of T>C reads was assessed with a Mann–Whitney *U* test for each sample as initially described in the alleyoop snpeval toolchain module. For the reference set of 3′ UTRs, a genome feature file (GFF3) for the *R. norvegicus* genome (release 6.0) was downloaded from Ensembl release v97, filtered to retain only three_prime_utr features and converted to BED format using bedops v2.4.36. The BED file was used in combination with parameters '-c 1, -q 27' for the SLAMDUNK count command, leaving other parameters at default. Resulting 3′-UTR T>C and total read counts were added up on the gene level along all transcripts and alternative 3′ UTRs available per transcript. The entire downstream analysis was performed using R v3.6.1, data.table v1.12.2, and common tidyverse packages (tidyr, dplyr, purrr, stringr, ggplot2). Differential gene expression analysis was carried out using DESeq2 v1.26.0 on the T>C count and total count matrices separately with standard settings and the α level set to 0.05. In total, six DESeq2 experiments were performed, two with pooled time points (1 h + 6 h) per read type (design variables of treatment and time) and four with separate time points for each read type (design variable of treatment only). Effect size was calculated using implementation of Cohen's *d* from the effsize v0.7.6 package. Gene set enrichment and over-representation analyses were performed using GeneTrail 3.0 (ref. [65]). Category source databases were adjusted independently, and *P* values were corrected using the FDR-controlling procedure by Benjamini–Hochberg and considered significant if smaller than 0.05.

Isolation and sorting of oligodendrocyte nuclei

Isolation of nuclei from frozen dissected hippocampi was performed as previously described[66] using the Nuclei EZ Prep kit (Sigma-Aldrich). Following the final PBS wash, nuclei were pelleted and resuspended in 100 µl of antibody mix (1:100 anti-NeuN antibody-Alexa Fluor 647, EPR12763, and 1:100 anti-Olig2 antibody-Alexa Fluor 488) with 0.2 U μl^{-1} RNase inhibitor (Takara, 23138) in FACS buffer (0.5% BSA in PBS) and were incubated on ice with intermittent shaking for 30 min. Nuclei were washed with 1 ml FACS buffer and were pelleted by centrifugation at 500 RCF for 5 min, resuspended in FACS buffer with 0.2 U μl^{-1} RNase inhibitor and Hoechst 33342 (1:2,000; Thermo, H3570), sorted on a Sony Sorter (SH800) on the basis of $Hoechst^{+}NeuN^{-}Olig2^{high}$ (OPC) and $Hoechst^{+}NeuN^{-}Olig2^{low}$ (OL) gating to 350 µl of RTL buffer and stored at −80 °C until RNA extraction. Data were analysed using FlowJo software (TreeStar).

RT–qPCR

Oligodendrocyte nuclei were isolated by FACS, and RNA was extracted with the RNeasy Plus Micro kit (Qiagen, 74034). cDNA was generated with qScript cDNA SuperMix (QuantaBio, 95048). Samples were diluted and mixed with SYBR Green master mix before loading as technical triplicates for qPCR on a LightCycler 480 (Roche). $\Delta\Delta C_T$ values normalized to *Gapdh* were used to assess relative gene expression between samples. The following validated primer pair for mouse *Srf* were used: 5′-GGCCGCGTGAAGATCAAGAT-3′ (forward) and 5′-CACATGGCCTGTCTCACTGG-3′ (reverse).

Bulk RNA-seq

Hippocampal RNA-seq. Frozen dissected hippocampi were thawed on ice and homogenized in 350 µl RLT buffer by 20 strokes using a manual homogenizer, and total RNA was isolated with the RNeasy Plus Micro kit (Qiagen, 74034). RNA quantity and quality were assessed by Agilent 2100 Bioanalyzer (Agilent Technologies). All samples passed a quality-control threshold (RIN ≥ 9) to proceed to library preparation and RNA-seq on a HiSeq 4000 (Illumina) using paired-end 100-bp reads. Libraries were sequenced to a depth of >20 million reads per sample.

Raw sequencing files were demultiplexed with bcl2fastq, reads were aligned using STAR and counts for technical replicates were summed using DESeq2 before performing normalization and differential expression analysis with standard settings.

For deconvolution analysis of bulk RNA-seq data, we used the CIBERSORTx algorithm[67] to deconvolve the bulk RNA-seq data. First, we used single-nucleus RNA-seq data describing the brain of 3-month-old young mice[66] to construct a cell-type-specific signature matrix with CIBERSORTx. We sampled 100 cells equally across the following cell types: astrocytes, choroid plexus, endothelial cells (BEC), interneurons, microglia, neurons of the trisynaptic loop (neuron CA), neurons of the dentate gyrus (neuron DG), oligodendrocytes, oligodendrocyte precursors and pericytes. Sampling was done over the annotated, quality-controlled data provided by the authors of ref. [66] to ensure efficiency for CIBERSORTx. Next, we ran CIBERSORTx on this sampled and CPM-normalized dataset with default parameters and inferred a 'signature matrix' that provided gene signatures for each noted cell type. Next, by following ref. [68], we deconvolved CPM-normalized YM-CSF and aCSF samples separately in S-mode owing to the possibility of high technical variance. We conducted this step first to infer cell type fractions per sample. Next, we estimated cellular expression levels in 'group mode' to identify cell-type-specific gene expression profiles per condition group. Finally, we ran the differential expression code provided in ref. [68] comparing the cell-type-specific expression profiles estimated for YM-CSF and aCSF. *P* values were corrected with the Benjamini–Hochberg procedure (FDR = 0.05), and $\log_2$-transformed fold change values reflect changes in the estimated expression levels of each gene between YM-CSF and aCSF. Single-cell subsampling and single-cell data normalization were conducted with Python Scanpy 1.6.0 (ref. [69]). All CIBERSORTx-specific analyses were done with the web service of the CIBERSORTx team (https://cibersortx.stanford.edu/). Differential gene expression analysis was conducted in R 4.0.5.

RNA-seq of sorted OPCs. RNA was extracted with the RNeasy Plus Micro kit (Qiagen, 74034). cDNA synthesis and library preparation were performed in house using the Smart-seq2 protocol as previously described[70] (detailed protocol at https://doi-org.laneproxy.stanford.edu/10.17504/protocols.io.2uvgew6) with several modifications. Because of the low input of RNA content, 2 µl of RNA extracted from sorted nuclei was reverse transcribed using 16 cycles for OL samples and 18 cycles for OPC samples. Following bead clean-up using a 0.7× ratio with AMPure beads (Fisher, A63881), the cDNA concentration was measured using the Qubit 1× dsDNA HS kit (Q33231) and normalized to 0.4 ng µl^{-1} as input for library preparation. Then, 0.4 µl of each normalized sample was mixed with 1.2 µl of Tn*5* tagmentation mix (0.64 µl TAPS–PEG buffer (PEG 8000 (Promega, V3011) and TAPS-NaOH pH 8.5 (Boston Bioproducts, BB-2375)), 0.46 µl water and 0.1 µl Tn*5* enzyme (Illumina, 20034198), followed by incubation at 55 °C for 10 min. The reaction was stopped by adding 0.4 µl of 0.1% SDS (Fisher Scientific, BP166-500). Indexing PCR reactions were performed by adding 0.4 µl of 5 µM i5 indexing primer (IDT), 0.4 µl of 5 µM i7 indexing primer (IDT) and 1.2 µl of KAPA HiFi Non-Hot Start Master Mix (Kapa Biosystems) using 12 amplification cycles. Libraries were purified using two purification rounds with a ratio of 0.8× and 0.7× AMPure beads. Library quantity and quality were assessed using a Bioanalyzer (Agilent Technologies) and Qubit. All steps were done manually using eight-strip PCR tubes, and PCR reactions were carried out on a 96-well plate thermal cycler (Bio-Rad). Libraries were pooled and sequenced on a NextSeq 550 sequencer (Illumina) using single-end high-output 75-bp kit (Illumina, 20024906).

Libraries were sequenced to a depth of at least 10 million reads per sample. Raw sequencing files were demultiplexed, and known adaptor sequences were trimmed with bcl2fastq. Data analysis of raw sequencing data was performed using nextflow-core RNA-seq pipeline v3.0. In brief, the core workflow of the pipeline maps filtered reads against the species reference genome using STAR and computes transcript counts using RSEM. For nuclear RNA-seq data, a custom reference genome in which exon sequences in GTF files were modified to include all introns for each transcript was created and used for mapping instead. For mouse and rat sequencing data, the reference genomes GRCm38 and Rnor 6.0 provided by Illumina igenomes were used, respectively. All gene annotations were based on the Ensembl database. Obtained raw gene transcript counts for each sample were loaded into DESeq2, performing normalization for transcript length and sequencing depth, and differential expression analysis was performed with standard settings. Effect sizes for each gene were computed on the basis of normalized counts computed by DESeq2 using function cohen.d of the R package effsize. GSEA was performed using GeneTrail 3.0 using Benjamini–Hochberg FDR *P*-value adjustment with all remaining parameters kept at default.

Meta-analysis of SRF targets in single-cell datasets from the literature

For each dataset, gene counts, fold change values and adjusted *P* values calculated when comparing either case and control or old and young age groups were acquired from the publicly available supplementary tables of the corresponding publications[71–74]. Next, the list of SRF targets known in *Homo sapiens* (from the TRANSFAC dataset[75]) was mapped to orthologous gene identifiers in *Mus musculus* using the Ensembl database with release 100. The process described in the following was performed independently for OPC and mature oligodendrocyte clusters. For each dataset, the list of genes was intersected with the organism-matched list of SRF targets. Next, genes that did not pass the significance threshold for the adjusted *P* values at a cut-off of 0.05 were discarded from subsequent analysis. Finally, fold change values were normalized for each dataset to obtain a comparable scale and to mitigate project-dependent fluctuations in fold change due to varying sample counts.

Allen Brain Atlas analysis

For secondary analysis of Fgf17-positive cells and corresponding expression levels, we downloaded raw gene expression counts for two datasets from the Allen Brain Atlas data portal (https://portal.brain-map.org/). The first comprised human M1 cortex samples profiled with 10x 3′ gene expression yielding ~77,000 single-nucleus transcriptomes and the second comprised mouse hippocampus and cortex samples profiled with Smart-seq2 yielding ~77,000 single-cell transcriptomes. Each was loaded and analysed separately using the R programming language (v4.0.5) together with the packages Seurat (v4.0.6), SeuratWrappers (v0.3.0), bioconductor-mast (v1.16.0), monocle3 (v1.0.0), data.table (v1.14.2), lsa (v0.73.2), umap (0.2.7.0) and ggplot2 (v3.3.5). The official metadata and annotations provided were used to construct Seurat objects and dissect the data. A minimal number of 250 expressed features per cell and at least 100 cells detected per feature were enforced to filter the raw matrices. We then followed the official Seurat analysis workflow: normalization (step 1), selection of variable features using VST normalization and setting of the number of features to 2,000 (step 2), scaling and centring of informative features (step 3), principal-component analysis with 50 principal components (step 4), computation of the nearest-neighbour graph using 20 dimensions (step 5), identification of clusters in the graph when setting the resolution to 0.8 and the number of starts and iterations to 10 and 15, respectively (step 6), and UMAP-based dimension reduction with 20 input dimensions, the number of neighbours set to 30, the minimum distance set to 0.3 and the spread set to 1 (step 7). Fgf17-positive cells were defined by a normalized expression count larger than zero. For cell type cluster or region-specific analyses, the respective cells were extracted and analysis steps 2–7 from above were repeated. To compute enriched markers for the different subclusters, we used the FindAllMarkers function from Seurat together with the MAST package, requiring an absolute log-transformed fold change of at least 0.25 and a minimum

percentage expressed of 10%. To find a global transcriptome signature for the Fgf17-positive cells, we correlated the expression of *Fgf17* to that of all other expressed genes in selected clusters using the cosine similarity. Lists of genes ranked by decreasing correlation were then used to perform GSEA using GeneTrail 3.0.

Statistics and reproducibility

All non-RNA-seq analysis was done using GraphPad Prism 8 and 9 with the indicated statistical tests. Gene set enrichment and over-representation analyses were performed using GeneTrail 3.0 (ref. [76]). Category source databases were adjusted independently, and *P* values were corrected using the FDR-controlling procedure by Benjamini–Hochberg and considered significant if smaller than 0.05. Box plots show the median and 25th–75th percentile range, and the whiskers indicate values up to 1.5 times the interquartile range. In in vivo experiments with mice of the same age, mice were divided into groups to achieve a similar average weight across groups. All other criteria were not considered and, as such, were randomized. Data in Figs. 1b, e, i, k and 4l and Extended Data Fig. 1a–f are combined raw data from two independent cohorts of mice. Data in Figs. 1l–o, 2e, i and 4b, c, f, h, j, s and Extended Data Figs. 2b, 7a, b, d–f, h, i and 9a, b, d, e were successfully replicated in two independent experiments. Figure schematics were created with BioRender and Inkscape.

Reporting summary

Further information on research design is available in the Nature Research Reporting Summary linked to this paper.

Data availability

All data are available in the main text or the Supplementary Information. Raw and processed sequencing data were deposited to NCBI's Sequence Read Archive and Gene Expression Omnibus databases using accession code GSE198008.

Code availability

All analyses were carried out using freely available software packages. Custom code used to analyse the RNA-seq data and datasets generated and/or processed in the current study is available from the corresponding authors on request.

51. De Miguel, Z. et al. Exercise plasma boosts memory and dampens brain inflammation via clusterin. *Nature* **600**, 494–499 (2021).
52. Liu, L. & Duff, K. A technique for serial collection of cerebrospinal fluid from the cisterna magna in mouse. *J. Vis. Exp.* https://doi.org/10.3791/960 (2008).
53. Smith, A., Wu, A. H., Lynch, K. L., Ko, N. & Grenache, D. G. Multi-wavelength spectrophotometric analysis for detection of xanthochromia in cerebrospinal fluid and accuracy for the diagnosis of subarachnoid hemorrhage. *Clin. Chim. Acta* **424**, 231–236 (2013).
54. Olsson, M., Arlig, J., Hedner, J., Blennow, K. & Zetterberg, H. Sleep deprivation and cerebrospinal fluid biomarkers for Alzheimer's disease. *Sleep* https://doi.org/10.1093/sleep/zsy025 (2018).
55. Olsson, M., Arlig, J., Hedner, J., Blennow, K. & Zetterberg, H. Sleep deprivation and plasma biomarkers for Alzheimer's disease. *Sleep Med.* **57**, 92–93 (2019).
56. Lynch, H. J., Rivest, R. W. & Wurtman, R. J. Artificial induction of melatonin rhythms by programmed microinfusion. *Neuroendocrinology* **31**, 106–111 (1980).
57. Pluvinage, J. V. et al. CD22 blockade restores homeostatic microglial phagocytosis in ageing brains. *Nature* **568**, 187–192 (2019).
58. Lukinavicius, G. et al. Fluorogenic probes for live-cell imaging of the cytoskeleton. *Nat. Methods* **11**, 731–733 (2014).
59. Friedman, P. L. & Ellisman, M. H. Enhanced visualization of peripheral nerve and sensory receptors in the scanning electron microscope using cryofracture and osmium–thiocarbohydrazide–osmium impregnation. *J. Neurocytol.* **10**, 111–131 (1981).
60. Willingham, M. C. & Rutherford, A. V. The use of osmium–thiocarbohydrazide–osmium (OTO) and ferrocyanide-reduced osmium methods to enhance membrane contrast and preservation in cultured cells. *J. Histochem. Cytochem.* **32**, 455–460 (1984).
61. Ewald, A. J. et al. Mammary collective cell migration involves transient loss of epithelial features and individual cell migration within the epithelium. *J. Cell Sci.* **125**, 2638–2654 (2012).
62. McDonald, K. L. & Webb, R. I. Freeze substitution in 3 hours or less. *J. Microsc.* **243**, 227–233 (2011).
63. Emery, B. & Dugas, J. C. Purification of oligodendrocyte lineage cells from mouse cortices by immunopanning. *Cold Spring Harb. Protoc.* **2013**, 854–868 (2013).
64. Muhar, M. et al. SLAM-seq defines direct gene-regulatory functions of the BRD4–MYC axis. *Science* **360**, 800–805 (2018).
65. Stockel, D. et al. Multi-omics enrichment analysis using the GeneTrail2 web service. *Bioinformatics* **32**, 1502–1508 (2016).
66. Hahn, O. et al. CoolMPS for robust sequencing of single-nuclear RNAs captured by droplet-based method. *Nucleic Acids Res.* **49**, e11 (2021).
67. Newman, A. M. et al. Determining cell type abundance and expression from bulk tissues with digital cytometry. *Nat. Biotechnol.* **37**, 773–782 (2019).
68. Steen, C. B., Liu, C. L., Alizadeh, A. A. & Newman, A. M. Profiling cell type abundance and expression in bulk tissues with CIBERSORTx. *Methods Mol. Biol.* **2117**, 135–157 (2020).
69. Wolf, F. A., Angerer, P. & Theis, F. J. SCANPY: large-scale single-cell gene expression data analysis. *Genome Biol.* **19**, 15 (2018).
70. Schaum, N. et al. Ageing hallmarks exhibit organ-specific temporal signatures. *Nature* **583**, 596–602 (2020).
71. Spitzer, S. O. et al. Oligodendrocyte progenitor cells become regionally diverse and heterogeneous with age. *Neuron* **101**, 459–471 (2019).
72. Mathys, H. et al. Single-cell transcriptomic analysis of Alzheimer's disease. *Nature* **570**, 332–337 (2019).
73. Zhou, Y. et al. Human and mouse single-nucleus transcriptomics reveal TREM2-dependent and TREM2-independent cellular responses in Alzheimer's disease. *Nat. Med.* **26**, 131–142 (2020).
74. The Tabula Muris Consortium. A single-cell transcriptomic atlas characterizes ageing tissues in the mouse. *Nature* **583**, 590–595 (2020).
75. Matys, V. et al. TRANSFAC and its module TRANSCompel: transcriptional gene regulation in eukaryotes. *Nucleic Acids Res.* **34**, D108–D110 (2006).
76. Gerstner, N. et al. GeneTrail 3: advanced high-throughput enrichment analysis. *Nucleic Acids Res.* **48**, W515–W520 (2020).

Acknowledgements We thank the members of the Wyss-Coray and Zuchero laboratories for feedback and support. Specifically, we thank H. Kantarci for advice on TEM tissue processing, imaging and analysis, H. Zhang and K. Dickey for laboratory management, and B. Carter for flow cytometry technical expertise. We thank V. Galata for graphical abstract design. We thank E. Mignot and J. Dalmau for providing human CSF samples. We also thank D. Jorgens and the staff at the University of California–Berkeley Electron Microscope Laboratory for EM sample preparation and data collection. This work was funded by the Department of Veterans Affairs (T.W.-C.), the National Institute on Aging (RF1-AG064897-02 to T.W.-C., T32AG000266 to M.S.H.), the NOMIS Foundation (T.W.-C.), the Nan Fung Life Sciences Aging Research Fund (T.W.-C.), the Glenn Foundation for Aging Research (T.W.-C.), the Big Idea Brain Rejuvenation Project and Interdisciplinary Scholar fellowship from the Wu Tsai Neurosciences Institute (T.W.-C. and T.I.), the Zuckerman STEM leadership fellowship and Tel Aviv University President Award for women postdoctoral scholars (T.I.), the National MS Society Harry Weaver Neuroscience Scholar Award (J.B.Z.), the McKnight Scholar Award (J.B.Z.), the Myra Reinhard Family Foundation and the National Institutes of Health (R01-NS119823 to J.B.Z.). H.Z. is a Wallenberg Scholar supported by grants from the Swedish Research Council (2018-02532), the European Research Council (681712), Swedish State Support for Clinical Research (ALFGBG-720931), the Alzheimer Drug Discovery Foundation (ADDF), USA (201809-2016862) and the UK Dementia Research Institute at UCL.

Author contributions T.I. and T.W.-C. conceptualized the study. T.I. performed all surgical procedures. A. Kaur, S.M., H.S. and T.I. performed and analysed histology and cell culture experiments. A. Kaur, L.Y., J.L. and T.I. designed and performed behaviour experiments. S.M. performed SLAMseq experiments, which were designed and analysed by F.K. and T.I. A.R.M. and T.I. performed nuclei sorting and RNA-seq experiments with guidance from N.L. and O.H. F.K. and T.I. analysed the datasets. M.A.G. isolated OPCs from mice with *loxP*-flanked *Srf*, and M.I. and M.S.H. assisted with cell culture experiments. A.C.Y., A.R.M. and T.I. preformed labelled CSF and Fgf17 experiments. S.R.S. assisted with CSF collection. R.P. and B.L. assisted with bioinformatic analysis. H.Z. provided human CSF samples. T.I. wrote the manuscript with input from all authors, T.I. and F.K. designed manuscript figures, and J.B.Z. and T.W.-C. edited the manuscript. A. Keller, J.B.Z. and T.W.-C. supervised the work.

Competing interests T.W.-C. and T.I. are co-inventors on a patent application related to the work published in this paper (STDU2-39617.101, S21-153-Methods and compositions for improved memory in the aging). H.Z. has served at scientific advisory boards and/or as a consultant for Abbvie, Alector, Annexon, Artery Therapeutics, AZTherapies, CogRx, Denali, Eisai, Nervgen, Novo Nordisk, Passage Bio, Pinteon Therapeutics, Red Abbey Labs, Roche, Samumed, Siemens Healthineers, Triplet Therapeutics and Wave, has given lectures in symposia sponsored by Cellectricon, Fujirebio, Alzecure, Biogen and Roche, and is a cofounder of Brain Biomarker Solutions in Gothenburg AB (BBS), which is a part of the GU Ventures Incubator Program (outside the scope of the submitted work).

Additional information

Supplementary information The online version contains supplementary material available at https://doi.org/10.1038/s41586-022-04722-0.

Correspondence and requests for materials should be addressed to Tal Iram or Tony Wyss-Coray.

Peer review information *Nature* thanks Klaus-Armin Nave and the other, anonymous, reviewer(s) for their contribution to the peer review of this work. Peer reviewer reports are available.

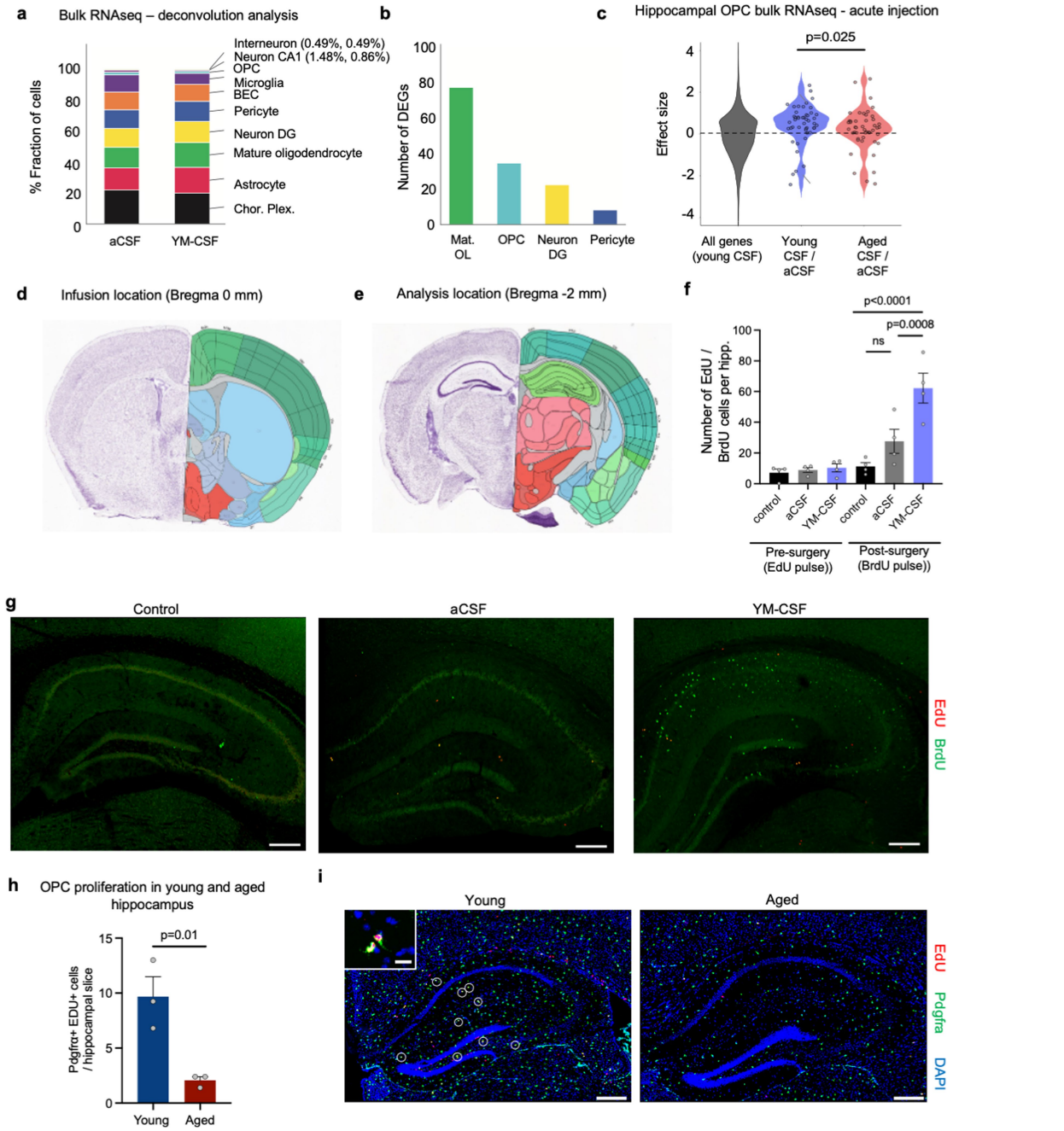

Extended Data Fig. 1 | Bulk RNAseq, infusion site details and overall overview of proliferating cells. a, Relative proportions of cell types as predicted by deconvolution analysis of bulk RNAseq of aged mice infused with aCSF or YM-CSF (aCSF n = 8, YM-CSF n = 7). **b**, Predicted number of DEGs per cell type by deconvolution analysis of bulk RNAseq of aged mice infused with aCSF or YM-CSF (aCSF n = 8, YM-CSF n = 7). **c**, Effect size of the subset of oligodendrocyte genes in Fig. 1d 16 h following acute injection of YM-CSF or aged mouse CSF (AM-CSF) calculated over aCSF as control (n = 4; Wilcoxon rank sum test). **d**, Location of infusion site. Image source: Allen Institute, Mouse brain atlas (coronal). **e**, Location of analysis site. Image source: Allen Institute, Mouse brain atlas (coronal). **f**, Hippocampal slice of 10-month-old mice given an EdU pulse prior to surgery showing low baseline proliferation, and three pulses of BrdU at day 5 and 6 of infusion showing an overall increase in proliferating cells following YM-CSF infusion (n = 4 per group; repeated measures two-way ANOVA followed by Sidak's post-hoc test; Means ± SEM). **g**, Representative images of EdU (red) and BrdU (green) cells in mice with no surgery or infused with aCSF or YM-CSF. Scale bar, 500 µm. **h**, RNAscope of Pdgfrα+EdU+ cells in hippocampus of 2-month-old (young) and 19-month-old (aged) mice (n = 3; two-sided *t*-test; mean ± s.e.m.). **i**, Representative images of analysis in panel h. Arrows pointing to Pdgfrα+EdU+ cells. Scale bar, 100 µm.

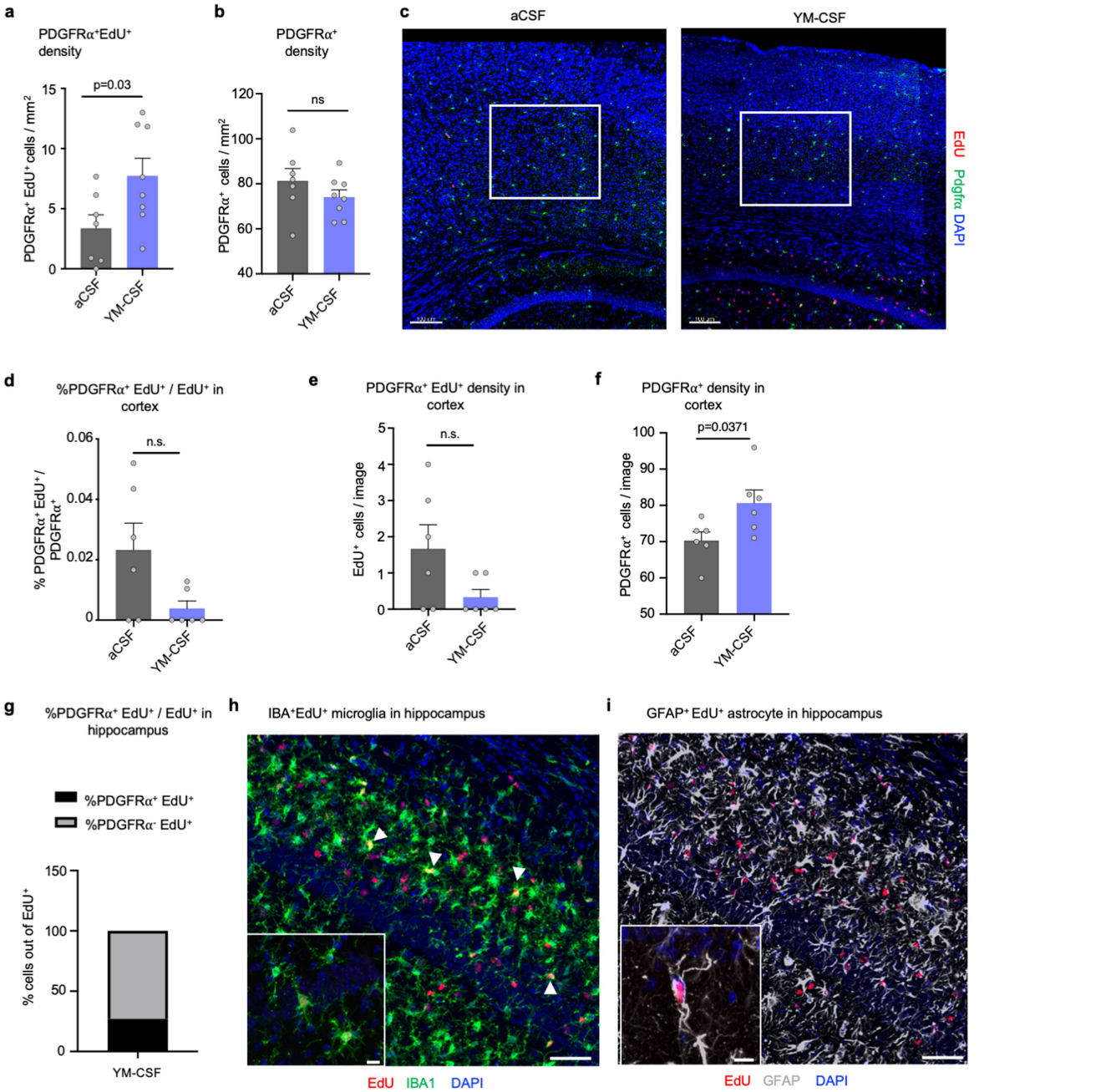

Extended Data Fig. 2 | Cortical Pdgfrα$^+$EdU$^+$ cells and identity of Pdgfrα$^-$ EDU$^+$ cells. a, Hippocampal density of Pdgfrα$^+$ EdU$^+$ cells per mm^2 (aCSF n = 7, YM-CSF n = 8; two-sided *t*-test; mean ± s.e.m.). **b**, Hippocampal density of Pdgfrα$^+$ cells per mm^2 (aCSF n = 7, YM-CSF n = 8; two-sided *t*-test; mean ± s.e.m.). **c**, Location of region of interest in the cortex. Scale bar, 100 µm. **d**, Percentage of Pdgfrα$^+$ EdU$^+$ / Pdgfrα$^+$ cells showing very low proliferation rates of OPCs in the cortex (n = 6; two-sided *t*-test; mean ± s.e.m.). **e**, Cortical density of Pdgfrα$^+$ EdU$^+$ cells per mm^2 (n = 6; two-sided *t*-test; mean ± s.e.m.). **f**, Cortical density of Pdgfrα$^+$ cells per mm^2 (n = 6; two-sided *t*-test; mean ± s.e.m.). **g**, Percentage of Pdgfrα$^+$ EdU$^+$ / EdU$^+$ in the hippocampus of aged mice infused with YM-CSF (n = 3). **h**, Example of IBA$^+$ EdU$^+$ cells in the hippocampus (n = 3). Scale bar, 50 µm. Insert, 10 µm. **i**, Example of GFAP$^+$ EdU$^+$ cells in the hippocampus (n = 3). Scale bar, 50 µm. Insert, 10 µm.

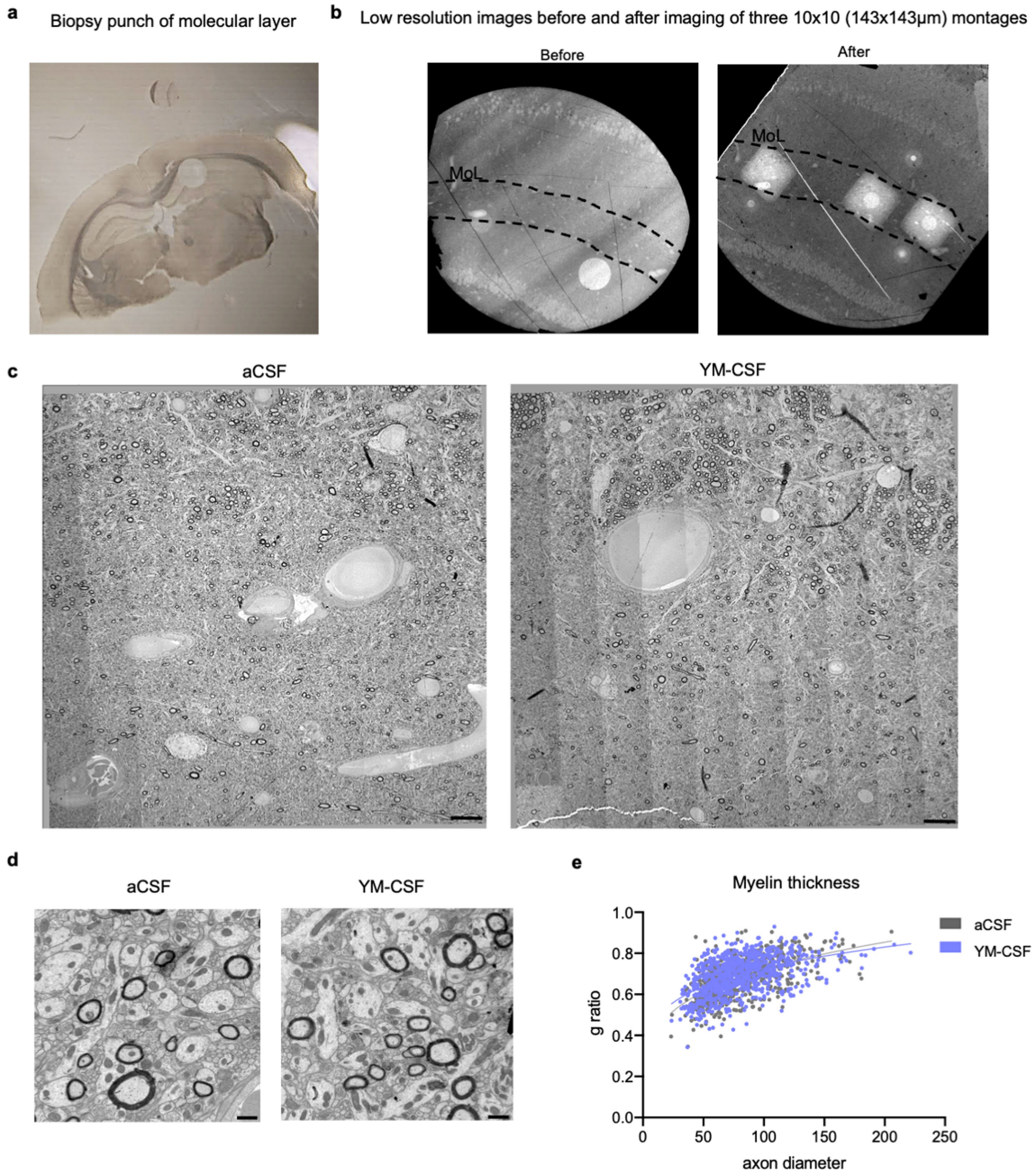

Extended Data Fig. 3 | Young CSF increases number of myelinated axons in the molecular layer. a, Representative overview of 1mm diameter biopsy punch in the hippocampus. **b**, Representative overview of molecular layer (MoL, between dashed lines) before and after TEM imaging of three 10x10 montage squares (n=7). **c**, Representative montage of MoL of aged mouse infused with aCSF and YM-CSF (n = 7). Scale bar, 10 µm. **d**, Representative higher resolution image of aged mouse infused with aCSF and YM-CSF (n = 7). Scale bar, 1 µm. **e**, g-ratio analysis of myelinated axons in molecular layer. (n = 3 mice per group, aCSF n = 321 axons, YM-CSF n = 291 axons).

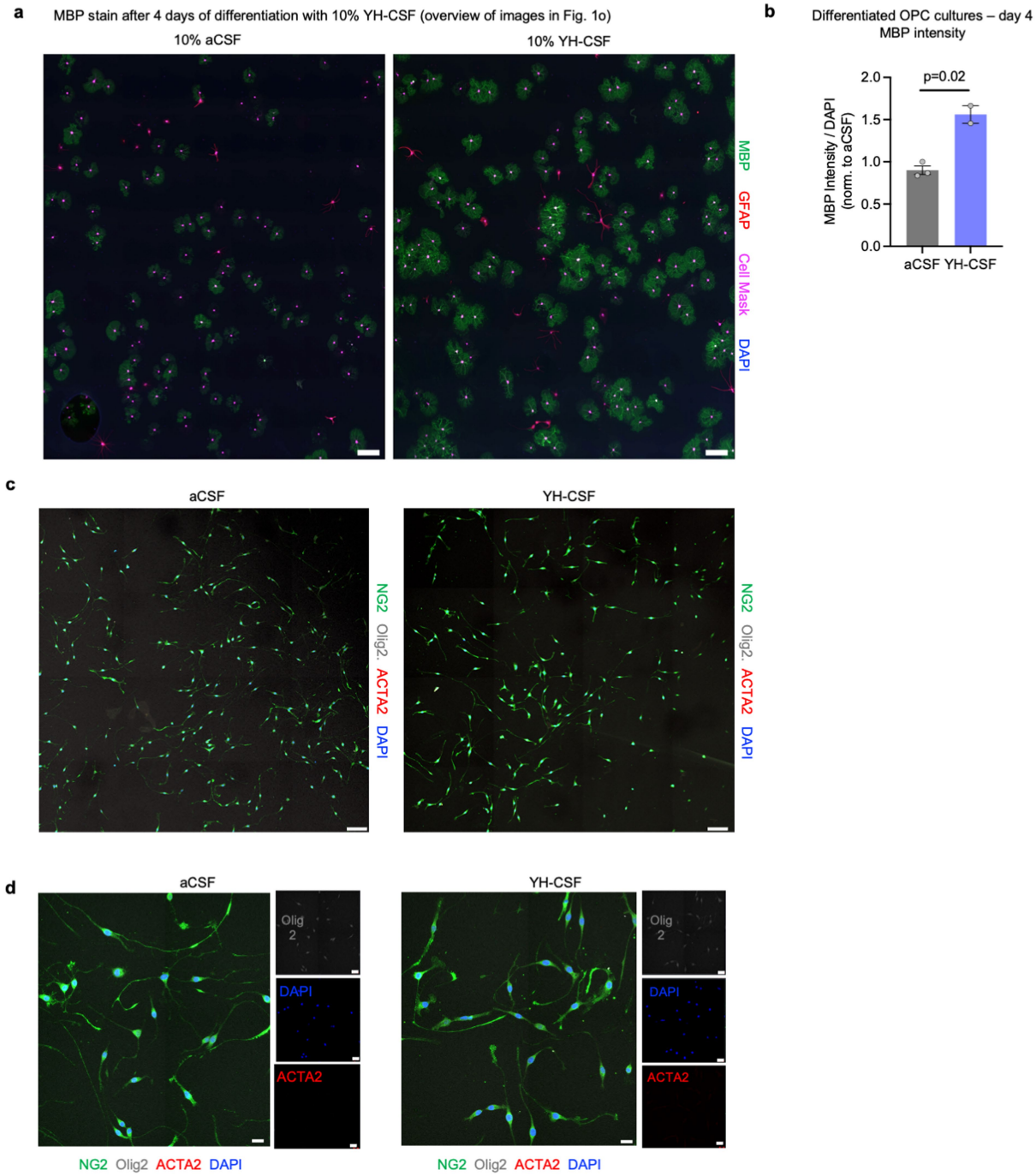

Extended Data Fig. 4 | Young CSF boosts OPC differentiation *in vitro* and validation of OPC culture purity. a, Related to images in Fig 1o. Overview of MBP stain of OLs at day 4 of differentiation supplemented with 10% aCSF or YH-CSF (aCSF n = 3 coverslips, YH-CSF n = 2 coverslips). **b**, Quantification of MBP intensity of day 4 differentiated OLs. Scale bar, 200 µm. (aCSF n = 3 coverslips, YH-CSF n = 2 coverslips; two-sided *t*-test; mean ± s.e.m). **c**, Primary rat OPC cultures were supplemented with 10% aCSF or YH-CSF for 6 h and stained for NG2 (green), Olig2 (grey) and Acta2 (red). (n = 3 coverslips; Scale bar, 100 µm). **d**, Higher magnification of primary rat OPC cultures were supplemented with 10% aCSF or YH-CSF for 6 h and stained for NG2 (green), Olig2 (grey) and Acta2 (red). (n = 3 coverslips; Scale bar, 20 µm).

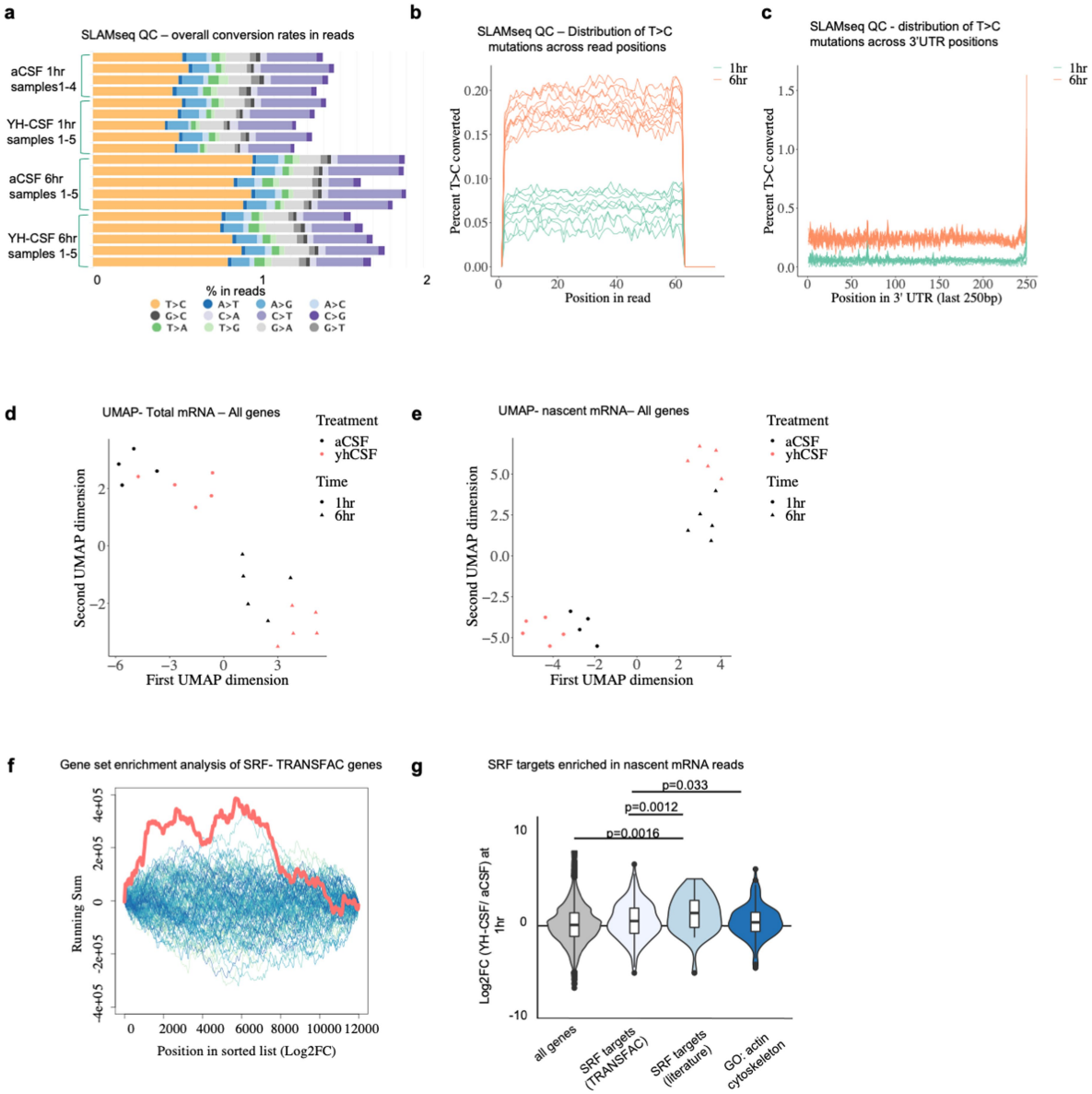

Extended Data Fig. 5 | SLAMseq QC and principal component analysis. **a**, Overall conversion rates in all SLAMseq samples, showing an enrichment for T>C mutation rate (orange bar) which increases with longer incubation time (6 h). **b**–**c**, Distribution of T>C mutations across **b**, read position and **c**, 3'UTR position indicating an equal distribution of s^4U incorporation along the positive strand. **d**–**e**, UMAP of aCSF and YH-CSF samples in both time points by all genes detected in the **d**, total and **e**, nascent mRNA counts. (young CSF 1 h n = 4, all the rest n = 5). **f**, Gene set enrichment analysis (GSEA) of 6hr genes sorted by log2FC showing an enrichment for SRF target genes by TRANSFAC[75]. **g**, Overall log2FC enrichment indicating upregulation of SRF target genes (TRANSFAC and curated list) and actin cytoskeleton genes in YH-CSF treated OPCs over aCSF. (SRF TRANSFAC (423 genes), validated SRF targets from literature (74 genes) and actin genes (212 genes); Wilcoxon rank sum test; box show the median and the 25–75th percentiles, and the whiskers indicate values up to 1.5-times the interquartile range).

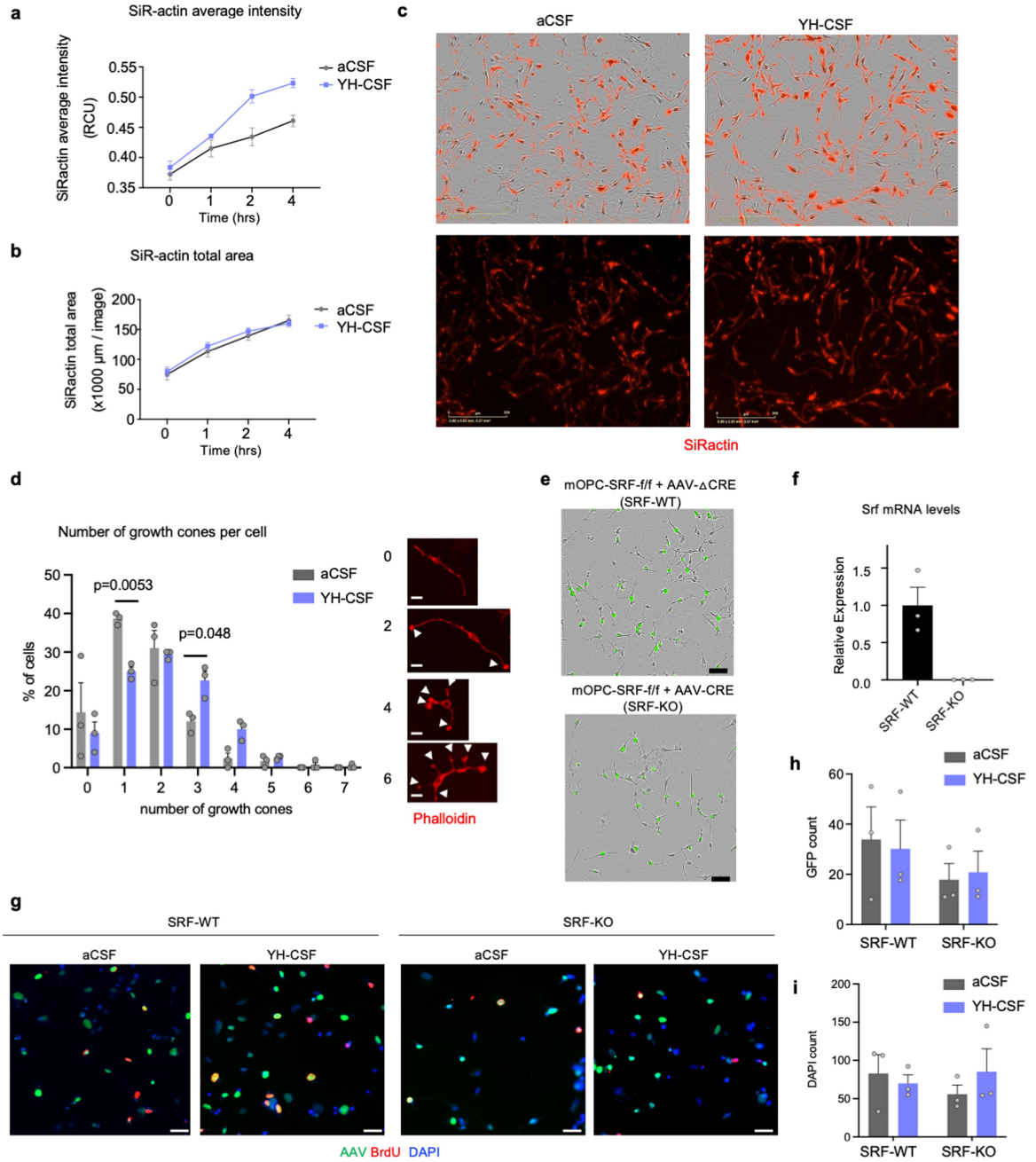

Extended Data Fig. 6 | YH-CSF induces actin cytoskeleton alterations *in vitro*. **a**–**b**, Actin filament content measured by live imaging using SiR-actin (red) throughout 4hr of aCSF and YH-CSF exposure. Average SiR-actin **a**, intensity and **b**, area in rat OPC cultures exposed to aCSF or YH-CSF (n = 6 wells per condition; Means ± SEM). **c**, Representative images of experiment quantified in panel a and b. Scale bar 200 µm. **d**, OPC coverslips were treated with YH-CSF for 6 h and stained for phalloidin. Histogram of the percentage of OPC with the indicated number of growth cones per cell. YH-CSF treated cells show a shift towards more growth cones per cell (n = 3 coverslips per condition, total of 200 cells analyzed per condition; two-way ANOVA followed by Sidak's post-hoc test; Means ± SEM). Scale bar 20 µm. **e**, mouse OPC primary cultures from SRF-fl/fl pups infected with CRE-GFP and △CRE-GFP AAVs to induce recombination. Representative images of infected cells (green) 48 h after infection. Scale bar, 100 µm. **f**, Normalized SRF mRNA levels as measured by RT-PCR (n = 3 coverslips per condition; mean ± s.e.m.). **g**, Representative image of data presented in figure 2h. Scale bar, 20 µm. **h**, Quantification of GFP$^+$ cells per image in SRF-WT and SRF-KO cells treated with 10% aCSF or YH-CSF. (n = 3; mean ± s.e.m.). **i**, Quantification of number of DAPI cells per image in SRF-WT and SRF-KO cells treated with 10% aCSF or YH-CSF. (n = 3; mean ± s.e.m.). Data in panels a-i were replicated in two independent experiments.

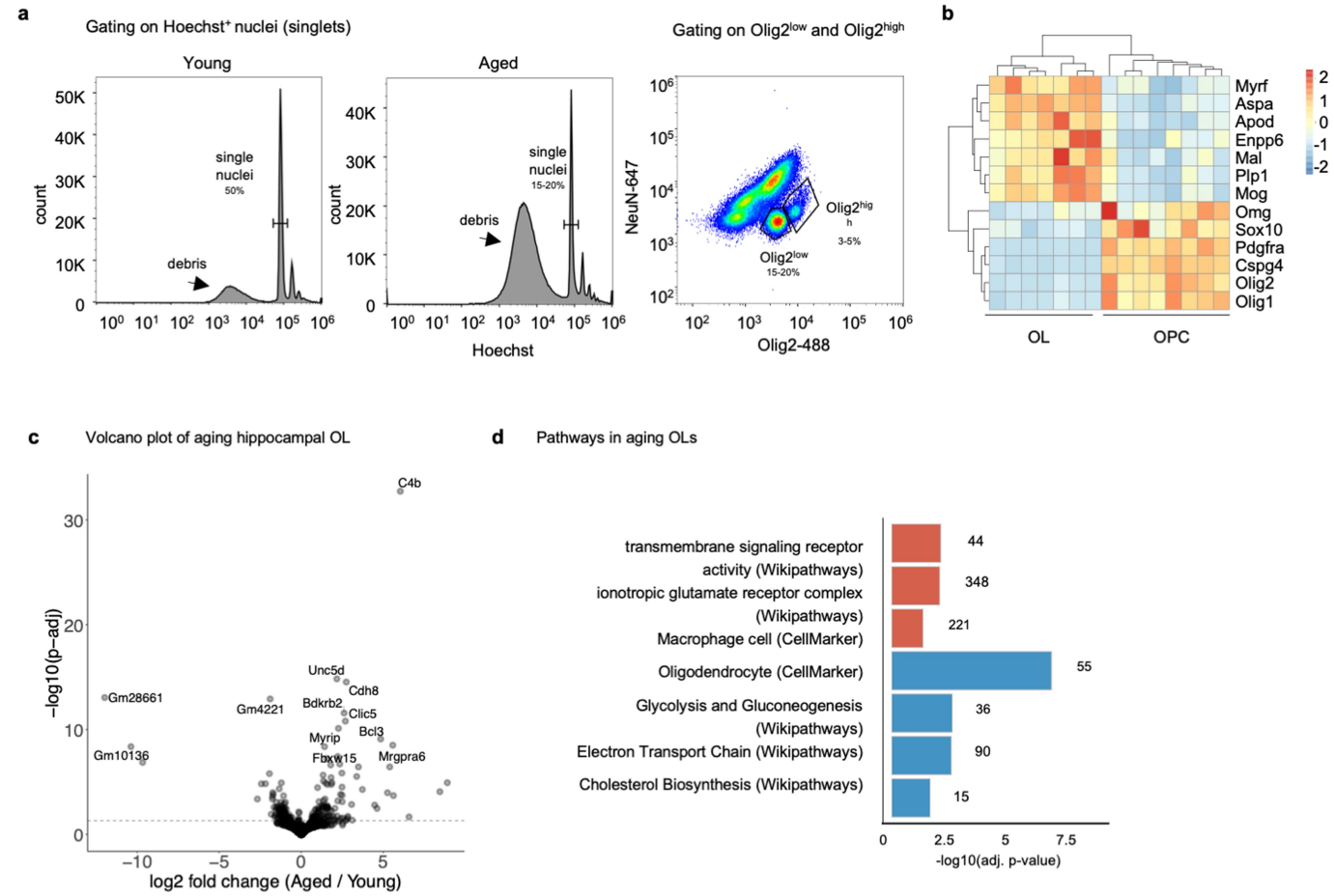

Extended Data Fig. 7 | Bulk RNAseq of hippocampal OPC and OL nuclei from young and aged mice. a, Gating strategy for sorting of hippocampal OPC and OL nuclei. **b**, Heatmap of expression OPC and OL specific genes across young and aged OPC and OL samples (aged OL n = 3, rest n = 4). **c**, Volcano plot showing OL genes up and downregulated with age (n = 4; p. adjusted value by Wald test in DESeq2). **d**, Pathways enriched (red) or depleted (blue) in hippocampal OLs with age (unweighted Kolmogorov-Smirnow test).

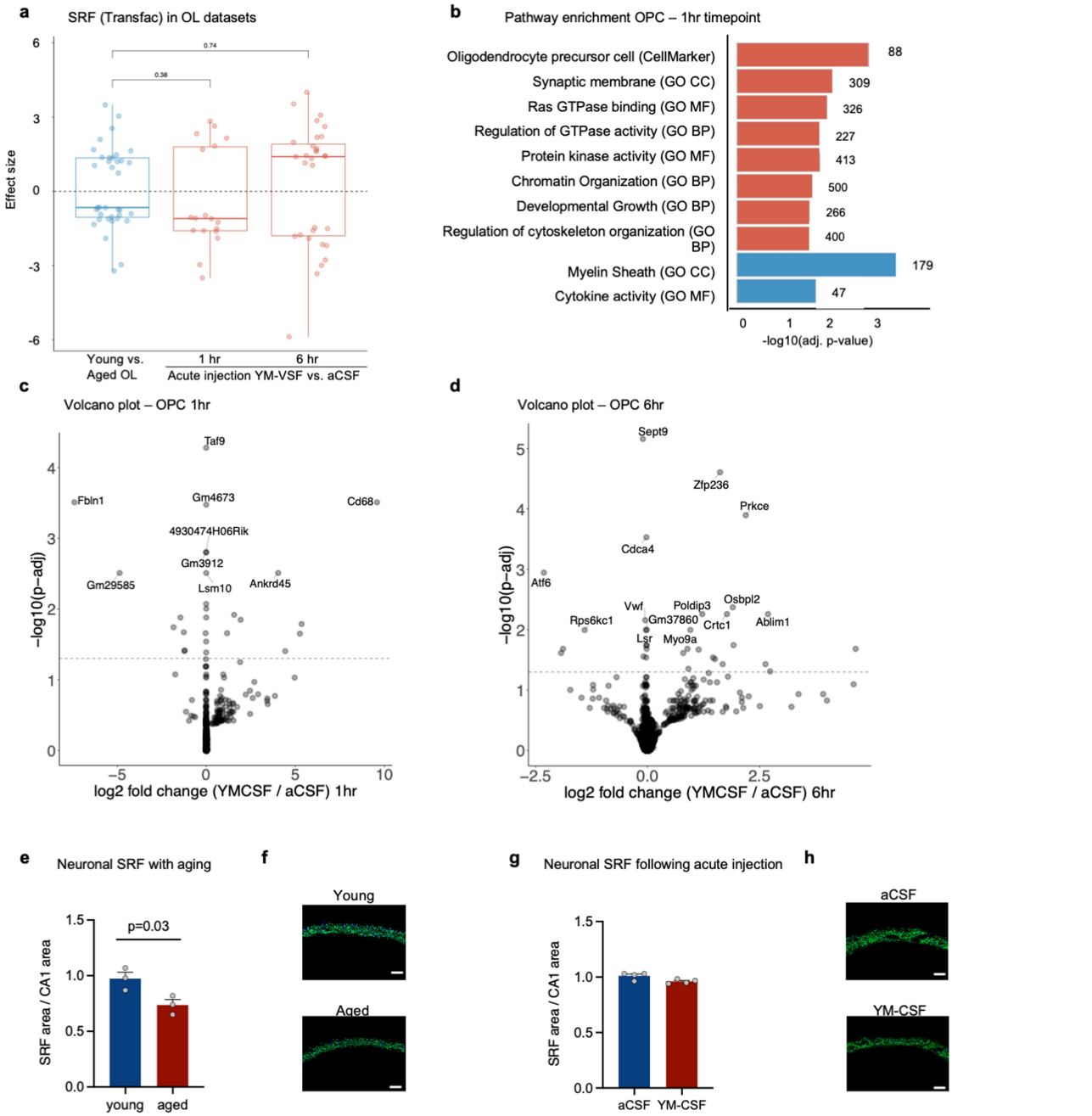

Extended Data Fig. 8 | Bulk RNAseq of hippocampal OPC and OL nuclei from aged mice following acute injection and Srf levels in neurons. a, Box plot of effect size of Srf targets (TRANSFAC database) in hippocampal OLs from aged vs. young, YM-CSF vs. aCSF at 1 h and 6 h timepoints (n = 4; genes pre-filtered by $p < 0.05$ cutoff; Wilcoxon rank sum test, box show the median and the 25–75th percentiles, and the whiskers indicate values up to 1.5-times the interquartile range). **b**, Pathways enriched (red) or depleted (blue) in hippocampal OPCs 1hr following injection of aCSF or YM-CSF (n = 4; p. adjusted value by Wald test in DESeq2). **c**, Volcano plot showing OPC genes up and down regulated 1hr following CSF injection (n = 4; p. adjusted value by Wald test in DESeq2). **d**, Volcano plot showing OPC genes up and down regulated 6hr following CSF injection (n = 4; p. adjusted value by Wald test in DESeq2). **e**, Neuronal Srf intensity in CA1 in young and aged mice. (n = 3; two-sided *t*-test; mean ± s.e.m). **f**, Representative image of panel e. Scale bar, 70 µm. **g**, Neuronal Srf intensity in CA1 in aged mice following YM-CSF infusion. (n = 4; two-sided *t*-test; mean ± s.e.m). **h**, Representative image of panel g. Scale bar, 70 µm.

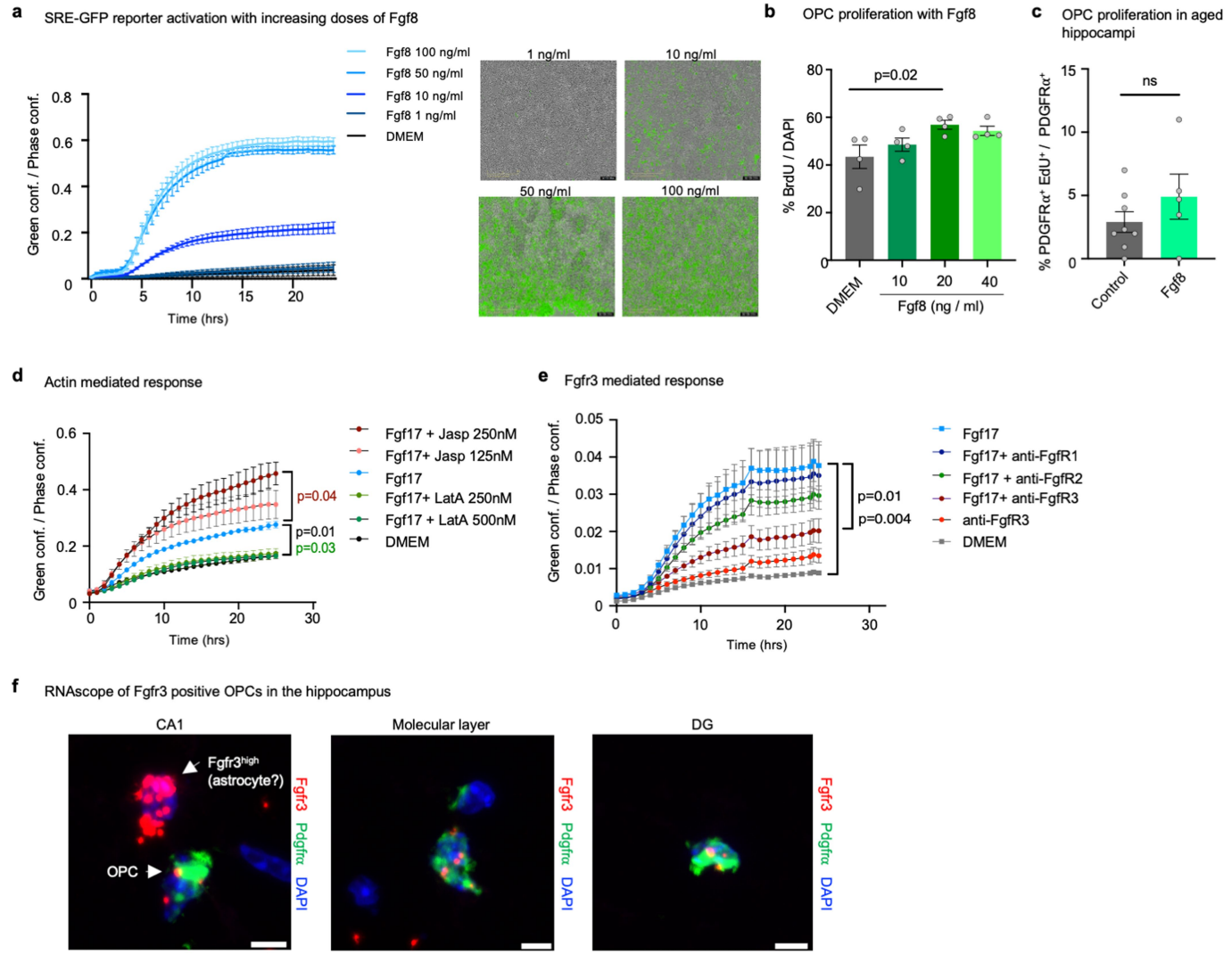

Extended Data Fig. 9 | Fgf8 induces OPC proliferation and Fgf17 induces SRF reporter activation mediated by actin dynamics and Fgfr3. **a**, Dose-dependent activation of SRE-GFP reporter by increasing concentrations of Fgf8 and representative images of the experiment at 15.5 h. Scale bar, 400 µm. (n = 3; similar control as in Fig. 4c; one-way ANOVA followed by Sidak's post-hoc test; mean ± s.e.m.). **b**, Percentage of BRDU$^+$/DAPI primary rat OPCs treated with 10, 20, 40 ng/ml Fgf8. (n = 4; one-way ANOVA followed by Tukey's post-hoc test; mean ± s.e.m.). **c**, Quantification of OPC proliferating cells (Pdgfrα$^+$EDU$^+$ / Pdgfrα$^+$ cells) in the CA1 region of the hippocampus of 20-month-old mice following a week of aCSF or Fgf8 infusion. (aCSF n = 8 similar control as in Fig. 4l, Fgf8 n = 4; two-sided *t*-test; mean ± s.e.m.). **d**, SRE-GFP activation with 200 ng/ml Fgf17 following 30 min pre-treatment with Jasplakinolide (Jasp, 125 or 250 nM) or Latrunculin A (LatA, 250 or 500 nM). (n = 3; Two-way ANOVA with Tukey's multiple comparisons test; mean ± s.e.m.). **e**, SRE-GFP activation with 200 ng/ml Fgf17 following 30 min pre-treatment with blocking antibodies for FgfR1, FgfR2, FgfR3 (all 50 µg/ml) or FgfR3 alone (n = 3; One-way ANOVA with Sidak's multiple comparisons test; mean ± s.e.m.). **f**, Example of Pdgfrα$^+$ Fgfr3$^+$ cells in the hippocampus of young mice. (n = 3). Scale bar, 5 µm.

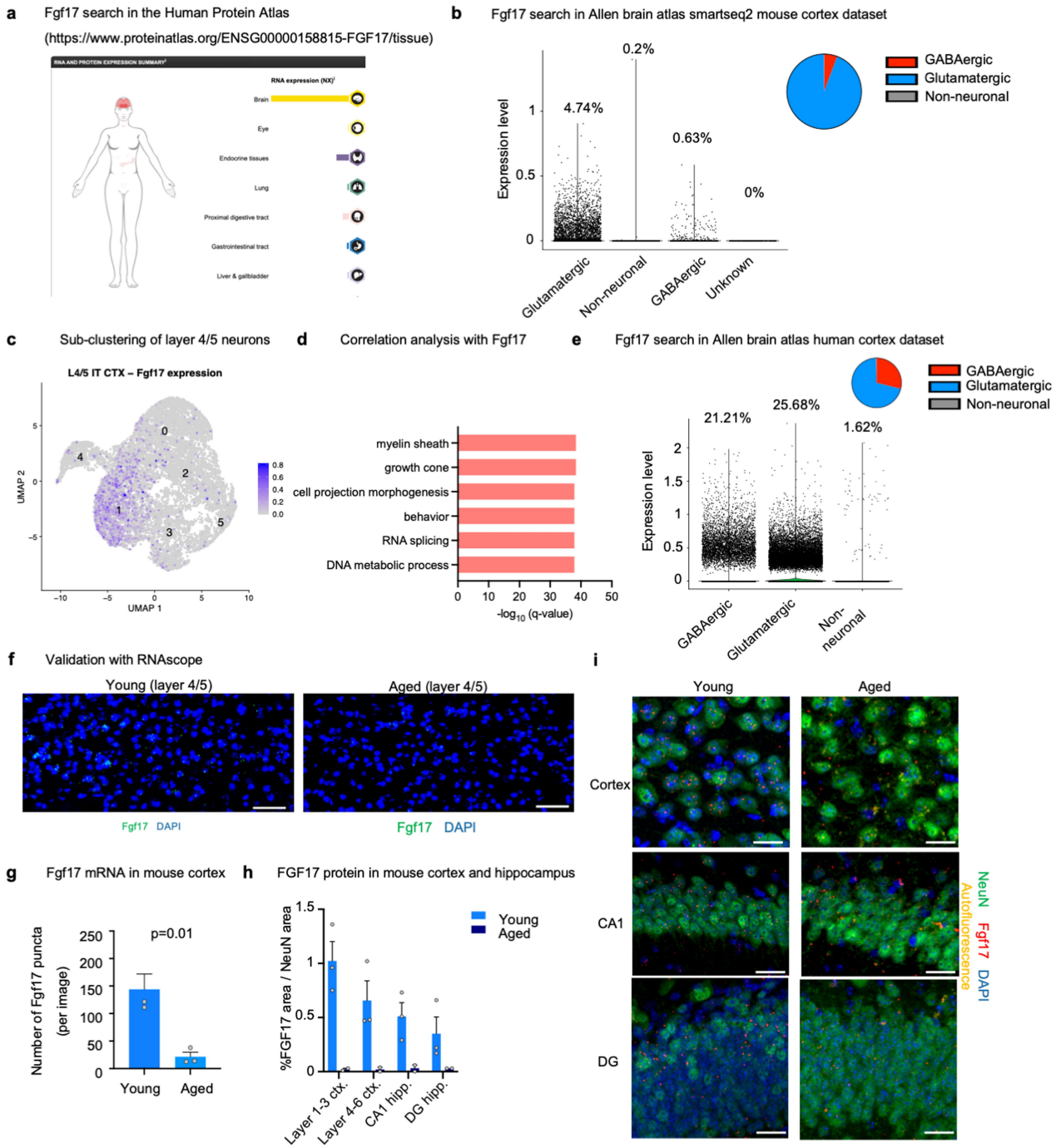

Extended Data Fig. 10 | Fgf17 is predominantly expressed in the brain by a subset of neurons and is downregulated with age. a, Fgf17 is predominantly expressed in the brain based on the human protein atlas. **b**, Fgf17 is expressed by cortical glutamatergic neurons in the young adult mouse (Allen brain atlas). **c**, Sub-clustering of mouse cortical layer 4/5 neurons indicates expression by a subset of cortical neurons (Allen brain atlas). **d**, Gene set enrichment analysis of genes mostly correlated with Fgf17 in layer 4/5 neurons (Allen brain atlas). **e**, Fgf17 is expressed by cortical glutamatergic and GABAergic neurons in the human cortex (Allen brain atlas). **f**, Representative image of analysis in panel **g**. Scale bar, 100 µm. **g**, Fgf17 mRNA expression in cortical neurons drops dramatically in aged mice. (n = 3; two-way student t-test; mean ± s.e.m.). **h**, Fgf17 protein expression in cortical and hippocampal neurons drops dramatically in aged mice. (n = 3; mean ± s.e.m.). **i**, Representative images of analysis in panel h and Fig. 4f. Scale bar, 20 µm.

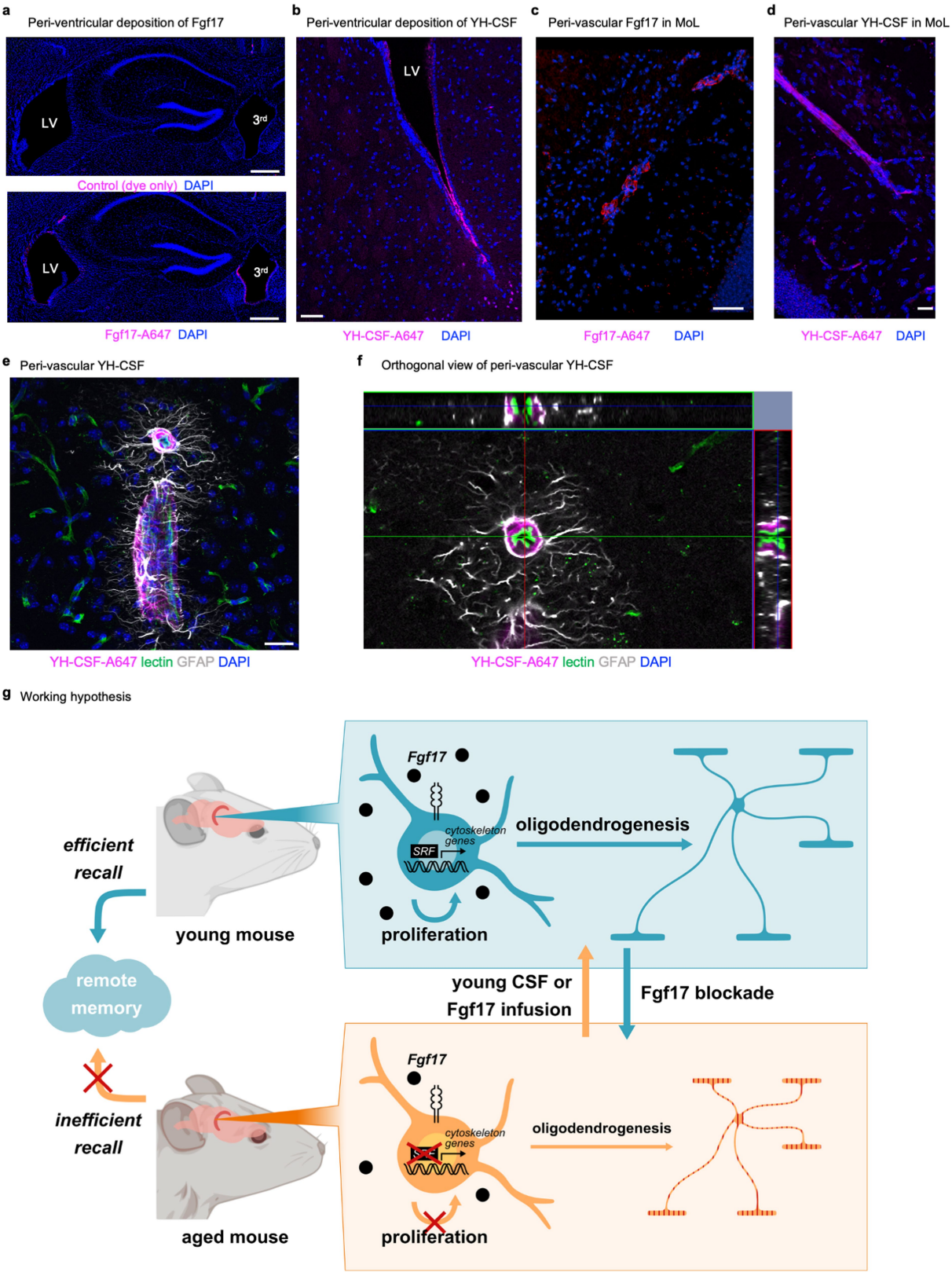

Extended Data Fig. 11 | Perfusion of labeled YH-CSF and mouse Fgf17 to the brain parenchyma and working model. a, Deposition of labeled Fgf17 on ventricular walls 3 h post ICV acute injection (n = 3). Scale bar, 300 µm. **b**, Deposition of labeled YH-CSF on lateral ventricle walls 2 h post ICV acute injection (n = 3). Scale bar, 100 µm. **c**, Labeled Fgf17 in perivascular spaces in the molecular layer of the hippocampus (n = 3). Scale bar, 50 µm. **d**, Labeled YH-CSF in perivascular spaces in the molecular layer of the hippocampus (n = 3). Scale bar, 20 µm. **e**, YH-CSF in the perivascular space in between the vessel (green) and astrocyte endfeet (white; n = 3). Scale bar, 20 µm. **f**, Orthogonal slice of YH-CSF (magenta) in perivascular space, in between the vessel (green) and astrocyte endfeet (white; n = 3). Scale bar, 20 µm. **g**, Working model. OPC proliferation and differentiation (termed oligodendrogenesis) slow down with age[40–43]. Re-exposure of the aged brain to young CSF or the brain-specific growth factor Fgf17[45], boost hippocampal oligodendorgenesis, concomitant with improvement in long term memory recall.

nature research

Corresponding author(s): Tony Wyss-Coray

Last updated by author(s): Mar 7, 2022

Reporting Summary

Nature Research wishes to improve the reproducibility of the work that we publish. This form provides structure for consistency and transparency in reporting. For further information on Nature Research policies, see our Editorial Policies and the Editorial Policy Checklist.

Statistics

For all statistical analyses, confirm that the following items are present in the figure legend, table legend, main text, or Methods section.

n/a	Confirmed	
☐	☒	The exact sample size (*n*) for each experimental group/condition, given as a discrete number and unit of measurement
☐	☒	A statement on whether measurements were taken from distinct samples or whether the same sample was measured repeatedly
☐	☒	The statistical test(s) used AND whether they are one- or two-sided *Only common tests should be described solely by name; describe more complex techniques in the Methods section.*
☐	☒	A description of all covariates tested
☐	☒	A description of any assumptions or corrections, such as tests of normality and adjustment for multiple comparisons
☐	☒	A full description of the statistical parameters including central tendency (e.g. means) or other basic estimates (e.g. regression coefficient) AND variation (e.g. standard deviation) or associated estimates of uncertainty (e.g. confidence intervals)
☐	☒	For null hypothesis testing, the test statistic (e.g. *F*, *t*, *r*) with confidence intervals, effect sizes, degrees of freedom and *P* value noted *Give P values as exact values whenever suitable.*
☒	☐	For Bayesian analysis, information on the choice of priors and Markov chain Monte Carlo settings
☐	☒	For hierarchical and complex designs, identification of the appropriate level for tests and full reporting of outcomes
☐	☒	Estimates of effect sizes (e.g. Cohen's *d*, Pearson's *r*), indicating how they were calculated

Our web collection on statistics for biologists contains articles on many of the points above.

Software and code

Policy information about availability of computer code

Data collection	FreezeScan tracking system (Cleversys), ZEN Black (Zeiss), Keyence microscope (BZ-X800), IncuCyte (Essen BioScience), SH800S (Sony), ImageStudio (LI-COR), Nextseq550 (Illumina), Hiseq 4000 (Illumina), LightCycler 480 (Roche).
Data analysis	Imaris 8 (Bitplane), FlowJo 10 (Treestar), Prism 8 and 9 (GraphPad), ImageJ/ Fiji (NIH), bcl2fastq v2.20.0.422, R v4 (DESeq2, ggplot2, tidyverse), STAR v2.6.1d, Nextflow v20.11.0-edge, nf-core/rnaseq pipeline v3.0, RSEM v1.3.1, Samtools v1.10, GeneTrail 3.0, SlamDunk v0.3.4, Snakemake v5.5.4. For the genome alignment reference fasta and gff files of GRCm38 (Mus musculus) and Rnor_6.0.97 (Rattus norvegicus) were downloaded from the Ensembl database. In case of aligning samples with high expected nuclear RNA content, we modified the gff files to account for intronic sequences and for determining the final read counts.

For manuscripts utilizing custom algorithms or software that are central to the research but not yet described in published literature, software must be made available to editors and reviewers. We strongly encourage code deposition in a community repository (e.g. GitHub). See the Nature Research guidelines for submitting code & software for further information.

Data

Policy information about availability of data

All manuscripts must include a data availability statement. This statement should provide the following information, where applicable:

- Accession codes, unique identifiers, or web links for publicly available datasets
- A list of figures that have associated raw data
- A description of any restrictions on data availability

All data is available in the main text or the supplementary materials. Raw and processed sequencing data were deposited to NCBI's SRA and GEO databases using the accession ID GSE198008.. Summarized bulk RNA-seq (Supp Table 1,2,4,5,6) are provided and meta analysis of publicly available datasets is referenced in the methods.

Field-specific reporting

Please select the one below that is the best fit for your research. If you are not sure, read the appropriate sections before making your selection.

☒ Life sciences ☐ Behavioural & social sciences ☐ Ecological, evolutionary & environmental sciences

For a reference copy of the document with all sections, see nature.com/documents/nr-reporting-summary-flat.pdf

Life sciences study design

All studies must disclose on these points even when the disclosure is negative.

Sample size	We used published data (Villeda, S.A. et al, 2011, Castellano, J.M. et al. 2017, De Miguel, Z. et al. 2021) to determine an optimal n for our studies on the effects of young CSF on behavior. For teh bulk RNAseq of sorted oligodendrocyte nuclei we performed preliminary studies to ensure we will capture enough nuclei for downstream library prep and statistical analysis.
Data exclusions	Animals were excluded from the experiments when showing an apparent state of disease, or died before the experiment finished. Mouse CSF samples were excluded for blood contamination using a cutoff of below 0.02 AU using the UV-vis setting with a 415nm wavelength for detection of oxyhemoglobin (see Methods).
Replication	For in vivo experiments, biological replicates (individual mice) are reported. Data in figure 1b, 1e, 1i, 1k, 4l and Extended data fig. 1a-f are combined raw data from two independent cohorts of mice as stated in 'Statistics and reproducibility' method section. Data in Fig. 1l-o, 2e, 2i, 4b-c, 4f, 4h, 4j and 4s and Extended data 2b, 7a, 7b, 7d, 7e, 7f, 7h, 7i, 9a, 9b, 9d, 9e, were successfully replicated in two independent experiments as stated in 'Statistics and reproducibility' method section RNA-seq data were not replicated in independent experiments due to resource restrictions.
Randomization	Same aged mice were allocated into groups to achieve an equal average weight. All other criteria were not considered and as such, were randomized.
Blinding	All behavioral and immunohistochemical analyses were performed by a blinded observer. In general, experimenters were blinded to group allocation during data acquisition and analysis.

Reporting for specific materials, systems and methods

We require information from authors about some types of materials, experimental systems and methods used in many studies. Here, indicate whether each material, system or method listed is relevant to your study. If you are not sure if a list item applies to your research, read the appropriate section before selecting a response.

Materials & experimental systems

n/a	Involved in the study
☐	☒ Antibodies
☐	☒ Eukaryotic cell lines
☒	☐ Palaeontology and archaeology
☐	☒ Animals and other organisms
☐	☒ Human research participants
☒	☐ Clinical data
☒	☐ Dual use research of concern

Methods

n/a	Involved in the study
☒	☐ ChIP-seq
☐	☒ Flow cytometry
☒	☐ MRI-based neuroimaging

Antibodies

Antibodies used	Flow cytometry: Anti-NeuN antibody-Alexa Fluor® 647 (1:100, abcam, EPR12763) and Anti-Olig2 antibody-Alexa Fluor® 488 (1:100, Millipore, MABN50A4). Immunostaining antibodies: PDGF Receptor α (D1E1E) XP® Rabbit mAb (1:500, Cell Signaling, 3174S), Rabbit-anti-MBP (1:100, MAB386, Millipore), Rat anti-BRDU antibody (1:500, ab6326, Abcam), Rabbit-anti-MBP (1:100, abcam, ab7349) and mouse anti-GFAP (1:500, Chemicon, MAB360), Rabbit anti-Fgf17 (1:500, PA5-109722, Thermo), goat anti-PROX1 (1:500, AF2727, R&D), rabbit anti-c-Fos (1:500, 9F6, Cell Signaling), Rabbit-anti-GFAP (Dako, Z0334, 1:500) RNAscope secondary antibodies: secondary Opal 690 and 520 reagents (FP1497001KT and FP1487001KT, Akoya Biosciences) were diluted at 1:1500 in TSA buffer.
Validation	All antibodies were validated for the indicated species and applications by the manufacturer.

Eukaryotic cell lines

Policy information about cell lines

Cell line source(s)	HEK293 (ATCC)
Authentication	Cell line was not authenticated.
Mycoplasma contamination	Cell line was not tested for mycoplasma contamination.
Commonly misidentified lines (See ICLAC register)	This study did not use any commonly misidentified lines

Animals and other organisms

Policy information about studies involving animals; ARRIVE guidelines recommended for reporting animal research

Laboratory animals	C57Bl/6 male mice, aged (18-22 months from NIA rodent colony), young (2-3 months from Charles River or Jackson Labs). Il of the mice were housed at the Palo Alto VA animal facility under a 12h–12h light–dark cycle with dark hours between 18:30–06:30, and housed at 68–73°F under 40–60% humidity.
Wild animals	This study did not involve wild animals
Field-collected samples	This study did not involve field-collected samples.
Ethics oversight	All animal care and procedures complied with the Animal Welfare Act and were in accordance with institutional guidelines and approved by the V.A. Palo Alto Committee on Animal Research and the institutional administrative panel of laboratory animal care at Stanford University.

Note that full information on the approval of the study protocol must also be provided in the manuscript.

Human research participants

Policy information about studies involving human research participants

Population characteristics	CSF samples of nine young heathy individuals (ages 24-26) were obtained through a collaboration with Dr. Henrik Zetterberg, University of Gothenburg, Sweden. The study was approved by the regional ethics committee at the University of Gothenburg and informed consent was obtained from all participants (Olssom, M et al. 2018, 2019). For in vitro experiments, three pools consisting of three individuals each were made for each experiment, two pools from six male samples and one of female samples were each used in 3-4 technical triplicates. Aged human CSF from healthy individuals (ages 65-76) was obtained from the Stanford Alzheimer's Disease Research Center.
Recruitment	The samples were baseline (normal sleep) lumbar CSF samples, collected in the morning, from healthy volunteers who took part in a study on sleep restriction-induced changes of CSF composition.
Ethics oversight	University of Gothenburg, Sweden. Stanford Alzheimer's Disease Research Center (ADRC), California, USA.

Note that full information on the approval of the study protocol must also be provided in the manuscript.

Flow Cytometry

Plots

Confirm that:

☒ The axis labels state the marker and fluorochrome used (e.g. CD4-FITC).

☒ The axis scales are clearly visible. Include numbers along axes only for bottom left plot of group (a 'group' is an analysis of identical markers).

☒ All plots are contour plots with outliers or pseudocolor plots.

☒ A numerical value for number of cells or percentage (with statistics) is provided.

Methodology

Sample preparation	Mouse hippocmapal nuclei were isolated using Nuclei EZ Prep Kit (Sigma-Aldrich, St. Louis, USA) and stained for 30 min on ice.
Instrument	SH800S (Sony)
Software	SH800S (Sony) and FlowJo (Treestar)

Cell population abundance	NeuN+ gate consisted of 50-60% of nuclei, Olig2-high were 5% and Olig2-low 20% of nuclei.
Gating strategy	Single nucei were gated by Hoechst staining (roughly 50% in young and 25% in aged). Olig2-high nuclei were sorted as OPCs and Olig2-low as mature oligodendrocytes. Fluorophores were chosen to minimize spectral overlap.

☒ Tick this box to confirm that a figure exemplifying the gating strategy is provided in the Supplementary Information.